# Dynamical model of $\phi$ meson photoproduction on the nucleon and $^4$He

Sang-Ho Kim [1,2,*] T.-S. H. Lee [3,†] Seung-il Nam [1,4,‡] and Yongseok Oh [5,4,§]

[1]*Department of Physics, Pukyong National University, Busan 48513, Korea*

[2]*Department of Physics and Origin of Matter and Evolution of Galaxy (OMEG) Institute, Soongsil University, Seoul 06978, Korea*

[3]*Physics Division, Argonne National Laboratory, Argonne, Illinois 60439, USA*

[4]*Asia Pacific Center for Theoretical Physics, Pohang, Gyeongbuk 37673, Korea*

[5]*Department of Physics, Kyungpook National University, Daegu 41566, Korea*

(Received 30 August 2021; accepted 6 October 2021; published 18 October 2021)

We investigate $\phi$ meson photoproduction on the nucleon and $^4$He targets within a dynamical model approach based on a Hamiltonian which describes the production mechanisms by the Pomeron exchange, meson exchange, $\phi$ radiation, and nucleon resonance excitation mechanisms. The final $\phi N$ interactions are included and described by the gluon-exchange, direct $\phi N$ couplings, and the box diagrams arising from the couplings with $\pi N$, $\rho N$, $K\Lambda$, and $K\Sigma$ channels. The parameters of the Hamiltonian are determined by the experimental data of $\gamma p \to \phi p$ from the CLAS Collaboration. The resulting Hamiltonian is then used to predict the coherent $\phi$-meson production on the $^4$He targets by using the distorted-wave impulse approximation. For the proton target, the final $\phi N$ rescattering effects, as required by the unitarity condition, are found to be very weak, which supports the earlier calculations in the literature. For the $^4$He targets, the predicted differential cross sections are in good agreement with the data obtained by the LEPS Collaboration. The role of each mechanism in this reaction is discussed and predictions for a wide range of scattering angles are presented, which can be tested in future experiments.

DOI: 10.1103/PhysRevC.104.045202

## I. INTRODUCTION

Photoproduction of vector mesons from nuclei has been studied to investigate nuclear shadowing and the hadronic structure of the photon based on the vector-meson dominance (VMD) hypothesis [1–4]. This also offers a way to study the production mechanisms from neutrons [5] and the medium modification of vector-meson properties [6].

Most experiments performed through photon-nucleus scatterings have been for semi-inclusive $\phi$ photoproduction from several nuclei, which allows us, with the VMD hypothesis, to estimate the value of the $\phi N$ total cross sections [7,8]. Recently, exclusive $\phi$ meson photoproduction processes have been investigated at SPring-8 and the Thomas Jefferson National Accelerator Facility. The measurements for coherent and incoherent $\phi$ photoproduction from deuterium targets were reported in Refs. [9–13] and, for the first time, exclusive $\phi$ photoproduction from the $^4$He targets were observed [14,15]. In the present work, we focus on the reaction of

$$\gamma + {}^4\mathrm{He} \to \phi + {}^4\mathrm{He} \tag{1}$$

and analyze the data reported in Ref. [14].

Theoretical studies on coherent $\phi$ photoproduction from nuclei are rather scarce. Most studies are for the reactions with deuteron targets [16–21], but the processes with light nuclei have not been studied in detail. The purpose of the present work is to investigate $\phi$ photoproduction on nuclei targets within the Hamiltonian formulation utilized by the Argonne National Laboratory and Osaka University (ANL-Osaka) Collaboration [22,23].

In this approach we construct a model Hamiltonian with the parameters determined by the data of $\phi$ photoproduction on the nucleon targets. Earlier studies of vector-meson photoproduction were mainly in the very-high-energy region where the Regge phenomenology is applicable, which led to a fairly successful Pomeron exchange model [24]. In the near-threshold-energy region, however, the mechanisms arising from meson-exchanges and the excitation of nucleon resonances ($N^*$) in the $\phi N$ channel would give non-negligible contributions, as demonstrated in Refs. [25–29]. In the present work, we follow the model of Refs. [28,29] for the mechanisms of $\phi$ photoproduction.

The unitarity condition requires that the $\gamma N \to \phi N$ amplitude must include the $\phi N \to \phi N$ final-state interaction (FSI) as well. As shown in the literature [23,30–32], the FSI is crucial for extracting the nucleon resonances ($N^*$) parameters from the experimental data. In addition, the $\phi N \to \phi N$ reaction is essential for exploring the possible $\phi$-nucleus bound states, as predicted by lattice quantum chromodynamics (LQCD) calculations [33]. This also accounts for the FSI in the reaction of $\phi$ meson photoproduction on *nuclei*. In

*shkim@pknu.ac.kr
†tshlee@anl.gov
‡sinam@pknu.ac.kr
§yohphy@knu.ac.kr

 

the present work, we elaborate on the model for this reaction as well. For this end, we construct a model for $\phi N$ interactions. As possible sources for $\phi N$ interactions one may consider the gluon-exchange mechanism within quantum chromodynamics (QCD) as well as the diagrams arising from nonvanishing $\phi NN$ coupling. Another possibility is due to the decay processes of $\phi \to K\bar{K}$ and $\phi \to \pi\rho$ which then lead to interactions through $\phi N \to KY, \pi N, \rho N$. To leading order these interactions generate the box-diagram mechanisms for $\phi N$ scattering, which will be elaborated in the present work.

With a model Hamiltonian constructed by fitting the data of $\phi$ photoproduction on the nucleon, we investigate its production on nuclei within the multiple-scattering formulation [34]. By using the well-established factorization approximation, the photoproduction amplitude on a nucleus can be expressed in terms of the $\gamma N \to \phi N$ amplitude and a nuclear form factor. The final $\phi$-nucleus interactions can be calculated from an optical potential, which is calculated, in the leading order, from the $\phi N \to \phi N$ amplitude and nuclear form factor. We apply this approach to understand the data from the $^4$He targets reported by the LEPS Collaboration [14].

This paper is organized as follows: In Sec. II, we present the formulation of $\phi$ photoproduction on the nucleon. Our dynamical model for $\phi$ photoproduction from the nucleon will be presented and discussed as well. Section III is devoted to the discussion on the Born terms of the amplitudes of $\phi$ photoproduction on the nucleon. The FSI amplitude of the reaction is then investigated in Sec. IV, which completes our model for $\phi$ photoproduction on the nucleon. The formulation for the photoproduction on nuclei will be discussed in Sec. V, which allows us to calculate the cross sections of $\gamma\, ^4\text{He} \to \phi\, ^4\text{He}$. Our numerical results for the nucleon targets and for the $^4$He targets are presented in Sec. VI. Section VII contains a summary and discussion.

## II. DYNAMICAL MODEL OF $\gamma N \to \phi N$ REACTION

Following the dynamical formulation of Refs. [22,23], we first define the model Hamiltonian which can generate the $\gamma N \to \phi N$ reaction and the $\phi N \to \phi N$ final-state interaction. It is also necessary to include the mechanisms induced by the $\phi$ meson decays such as $\phi \to K\bar{K}$ and $\phi \to \rho\pi$, whose decay widths are large enough to lead to non-negligible coupled-channel effects arising from the one-meson-exchange mechanisms in $\phi N \to KY$, $\pi N$, $\rho N$ processes. We thus consider the following form of the Hamiltonian:

$$H = H_0 + B_{\phi N,\gamma N} + \Gamma_{N^*,\gamma N} + \Gamma_{N^*,\phi N} + \sum_{MB=K\Lambda,K\Sigma,\pi N,\rho N} (v_{MB,\phi N} + \text{H.c.}), \tag{2}$$

where $H_0$ is the free Hamiltonian of the system, $B_{\phi N,\gamma N}$ is the Born term consisting of the tree diagrams for the reaction of $\gamma N \leftrightarrow \phi N$, and $v_{MB,\phi N}$ is the one-meson-exchange potential for $\phi N \leftrightarrow MB$.

As illustrated in Fig. 1, the full amplitude for the $\gamma N \to \phi N$ reaction defined by the above Hamiltonian can be written as

$$T_{\phi N,\gamma N}(E) = B_{\phi N,\gamma N} + T^{\text{FSI}}_{\phi N,\gamma N}(E) + T^{N^*}_{\phi N,\gamma N}(E), \tag{3}$$

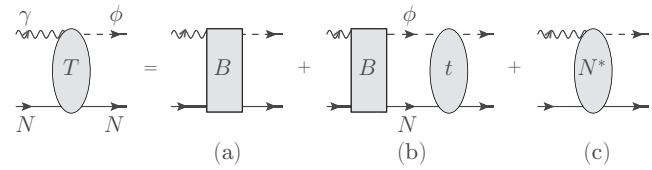


FIG. 1. Total amplitude of the $\gamma N \to \phi N$ reaction: $B$ is the production amplitude, $t$ is the $\phi N$ scattering amplitude, and $N^*$ is the nucleon resonance contributions.

where $T^{\text{FSI}}_{\phi N,\gamma N}(E)$ and $T^{N^*}_{\phi N,\gamma N}(E)$ are, respectively, the amplitudes due to the $\phi N$ final-state interactions and the $N^*$ contributions defined by the vertex functions $\Gamma_{N^*,\gamma B}$ and $\Gamma_{N^*,\phi N}$. Explicitly, we have

$$T^{\text{FSI}}_{\phi N,\gamma N}(E) = t_{\phi N,\phi N}(E) G_{\phi N}(E) B_{\phi N,\gamma N}, \tag{4}$$

where the meson-baryon propagator is

$$G_{MB}(E) = \frac{|MB\rangle\langle MB|}{E - H_0 + i\epsilon}. \tag{5}$$

The $\phi N \to \phi N$ scattering amplitude $t_{\phi N,\phi N}(E)$ in Eq. (4) is defined by

$$t_{\phi N,\phi N}(E) = V_{\phi N,\phi N}(E) + V_{\phi N,\phi N} G_{\phi N}(E) t_{\phi N,\phi N}(E), \tag{6}$$

where the $\phi N$ potential $V_{\phi N,\phi N}(E)$ is decomposed as

$$V_{\phi N,\phi N}(E) = v^{\text{Gluon}}_{\phi N,\phi N} + v^{\text{Direct}}_{\phi N,\phi N} + v^{\text{Box}}_{\phi N,\phi N}(E), \tag{7}$$

as illustrated in Fig. 2. Here, $v^{\text{Gluon}}_{\phi N,\phi N}$ is the gluon-exchange interaction [Fig. 2(a)] and $v^{\text{Direct}}_{\phi N,\phi N}$ is the direct $\phi N$ coupling term [Figs. 2(b) and 2(c)]. The box-diagram mechanisms [Figs. 2(d)–2(f)] are defined by

$$v^{\text{Box}}_{\phi N,\phi N}(E) = \sum_{MB} v_{\phi N,MB} G_{MB}(E) v_{MB,\phi N}, \tag{8}$$

where the intermediate meson-baryon ($MB$) states include the $K\Lambda$, $K\Sigma$, $\pi N$, $\rho N$ channels.

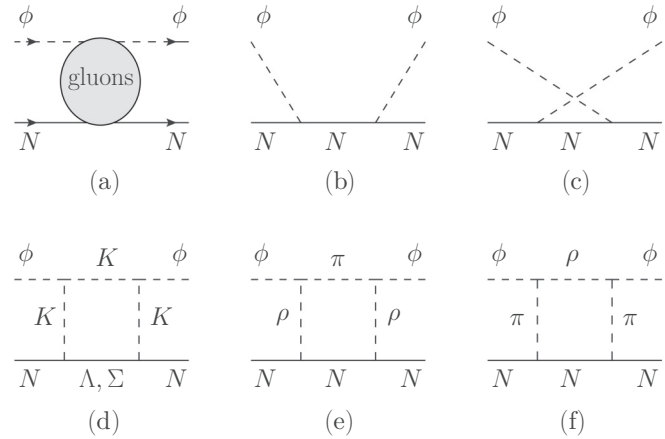


FIG. 2. Diagrams for the $\phi N \to \phi N$ interactions. (a) Gluon-exchange within QCD, (b), (c) mechanisms by the direct $\phi N$ coupling, and (d)–(f) box diagrams arising from the $\phi \to K\bar{K}$ and $\phi \to \pi\rho$ decays.

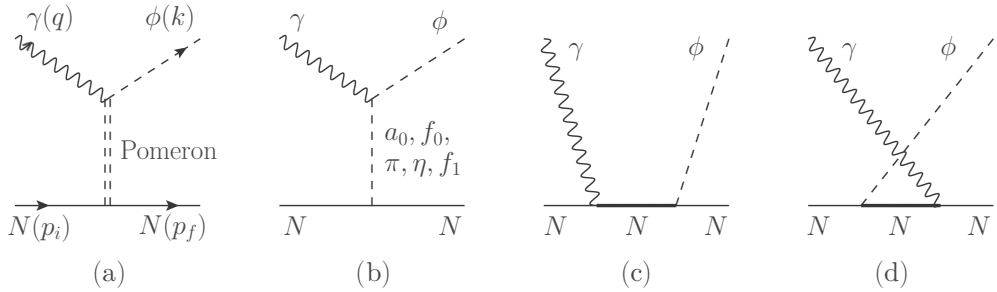


FIG. 3. Born terms of the $\gamma N \to \phi N$ reaction.

The $N^*$ excitation amplitude in Eq. (3) is

$$T^{N^*}_{\phi N,\gamma N}(E) = \sum_{N^*} \bar{\Gamma}^{\dagger}_{N^*,\phi N} \frac{1}{E - M_0^{N^*} - \Sigma_{N^*}(E)} \bar{\Gamma}_{N^*,\gamma N}, \quad (9)$$

where $\bar{\Gamma}_{N^*,MB}$ are the dressed vertices, $M_0^{N^*}$ is the bare mass of $N^*$, and $\Sigma_{N^*}(E)$ is the self-energy of $N^*$. The details of these dressed $N^*$ quantities are discussed in the next section.

By using the normalization condition $\langle \mathbf{k}|\mathbf{k}'\rangle = \delta^3(\mathbf{k} - \mathbf{k}')$ for plane-wave states [35] and $\langle \psi_B|\psi_B\rangle = 1$ for a single-particle state $\psi_B$, the differential cross section of $\gamma(q,\lambda_\gamma) + N(p_i, m_s) \to \phi(k,\lambda_\phi) + N(p_f, m_s')$ in the center-of-mass (c.m.) frame, where $\mathbf{p}_i = -\mathbf{q}$ and $\mathbf{p}_f = -\mathbf{k}$, can be written as

$$\frac{d\sigma}{d\Omega} = \frac{(4\pi)^2}{q^2} \rho_{\phi N}(W) \rho_{\gamma N}(W) \frac{1}{4} \sum_{\lambda_V, m_s'} \sum_{\lambda_\gamma, m_s} \times |\langle k\lambda_\phi; p_f m_s' | T_{\phi N,\gamma N}(W) | q\lambda_\gamma; p_i m_s\rangle|^2, \quad (10)$$

where

$$\rho_{\phi N} = \frac{k E_\phi(\mathbf{k}) E_N(\mathbf{k})}{W},$$
$$\rho_{\gamma N} = \frac{q^2 E_N(\mathbf{q})}{W}, \quad (11)$$

with $W = q + E_N(\mathbf{q}) = E_\phi(\mathbf{k}) + E_N(\mathbf{k})$ being the invariant mass. Here, $\lambda_\gamma$ and $\lambda_\phi$ are the helicities of the photon and the $\phi$ meson, respectively, and $m_s$ and $m_s'$ are the magnetic quantum numbers of the initial and final nucleons, respectively.

## III. BORN TERMS

In the present work, we model the Born terms of the $\gamma N \to \phi N$ reaction by the diagrams shown in Fig. 3, which defines the momenta of the involved particles as well. Depicted in Fig. 3(a) is the Pomeron exchange mechanism and we use the parametrization of Ref. [36] following the model of Donnachie and Lanshoff [37–40]. At low energies, however, the meson exchange mechanisms [Fig. 3(b)] and the direct $\phi$ radiations [Figs. 3(c) and 3(d)] may give nontrivial contributions. In the present work, we consider these mechanisms for constructing the $\gamma N \to \phi N$ reaction amplitudes.

The amplitude for the Born term can be written as

$$\langle k\lambda_\phi; p_f m_s' \mid B_{\phi N,\gamma N} \mid q\lambda_\gamma; p_i m_s\rangle = \frac{1}{(2\pi)^3} \sqrt{\frac{M_N^2}{4E_V(\mathbf{k}) E_N(\mathbf{p}_f) |\mathbf{q}| E_N(\mathbf{p}_i)}} \times [\bar{u}_N(p_f, m_s') \mathcal{M}^{\mu\nu}(k, p_f, q, p_i) u_N(p_i, m_s)] \times \epsilon_\nu^*(k,\lambda_\phi) \epsilon_\mu(q,\lambda_\gamma), \quad (12)$$

where $\epsilon_\mu(q,\lambda_\gamma)$ is the photon polarization vector with momentum $q$ and helicity $\lambda_\gamma$, and $\epsilon_\nu(k,\lambda_\phi)$ is that of the $\phi$ meson with momentum $k$ and helicity $\lambda_\phi$. The nucleon spinor of momentum $p$ and spin projection $m_s$ is represented by $u_N(p, m_s)$, which is normalized as $\bar{u}_N(p, m_s) u_N(p, m_s') = \delta_{m_s, m_s'}$. With the diagrams of Fig. 3, $\mathcal{M}^{\mu\nu}$ can be decomposed as

$$\mathcal{M}^{\mu\nu} = \mathcal{M}^{\mu\nu}_{\mathbb{P}} + \sum_{\Phi=\pi^0,\eta} \mathcal{M}^{\mu\nu}_{\Phi} + \sum_{S=a_0,f_0} \mathcal{M}^{\mu\nu}_{S} + \mathcal{M}^{\mu\nu}_{f_1} + \mathcal{M}^{\mu\nu}_{\phi,\mathrm{rad}}, \quad (13)$$

where $\mathcal{M}^{\mu\nu}_{\mathbb{P}}$ is from the Pomeron exchange, $\mathcal{M}^{\mu\nu}_{\Phi}$ from pseudoscalar meson exchanges, $\mathcal{M}^{\mu\nu}_{S}$ from scalar-meson exchanges, $\mathcal{M}^{\mu\nu}_{f_1}$ from $f_1(1285)$ axial-vector-meson exchange, and $\mathcal{M}^{\mu\nu}_{\phi,\mathrm{rad}}$ is from the direct $\phi$ radiations. In the following sections, each term of $\mathcal{M}^{\mu\nu}$ is discussed in detail.

### A. Pomeron exchange

Following Refs. [36,41,42], the production amplitude of the Pomeron-exchange mechanism for vector-meson photoproduction can be written in the form of

$$\mathcal{M}^{\mu\nu}_{\mathbb{P}}(k, p_f; q, p_i) = G_{\mathbb{P}}(s,t) \mathcal{T}^{\mu\nu}_{\mathbb{P}}(k, p_f; q, p_i), \quad (14)$$

where

$$\mathcal{T}^{\mu\nu}_{\mathbb{P}}(k, p_f; q, p_i) = i \frac{12 e M_V^2}{f_V} \beta_Q F_V(t) \beta_{u/d} F_1(t) (\not{q} g^{\mu\nu} - q^\nu \gamma^\mu), \quad (15)$$

with $t = (q-k)^2 = (p_f - p_i)^2$. Here, $e$ is the unit electric charge, $M_V$ is the vector-meson mass, and $f_V$ is the vector-meson decay constant. The empirical vector-meson decay constant for the $\phi$ meson is estimated as $f_V = 13.38$.[1]

[1]The value of $f_V$ is determined through the decay width of $\Gamma(V \to e^+e^-) = 4\pi M_V \alpha_{\mathrm{em}}/(3 f_V^2)$ with $\alpha_{\mathrm{em}} = e^2/(4\pi)$, which leads to

The coupling of the Pomeron with the quark $Q$ (or the antiquark $\bar{Q}$) in the vector meson $V$ is represented by $\beta_Q$ while that with the light quarks in the nucleon is given by $\beta_{u/d}$. The Pomeron–vector-meson vertex is dressed by the form factor

$$F_V(t) = \frac{1}{M_V^2 - t}\left(\frac{2\mu_0^2}{2\mu_0^2 + M_V^2 - t}\right). \tag{16}$$

By using the Pomeron-photon analogy advocated by Donnachie and Landshoff [37,44], the form factor for the Pomeron-nucleon vertex is assumed to be the isoscalar electromagnetic form factor of the nucleon, which can be written as

$$F_1(t) = \frac{4M_N^2 - 2.8t}{(4M_N^2 - t)(1 - t/0.71)^2}, \tag{17}$$

where $t$ is in units of GeV$^2$.

The crucial ingredient of the Regge phenomenology is in the propagator $G_{\mathbb{P}}$ of the Pomeron in Eq. (14), which takes the form

$$G_{\mathbb{P}} = \left(\frac{s}{s_0}\right)^{\alpha_P(t)-1} \exp\left\{-\frac{i\pi}{2}[\alpha_P(t) - 1]\right\}, \tag{18}$$

where $s = (q + p_i)^2 = W^2$ and $\alpha_P(t) = \alpha_0 + \alpha_P' t$. By fitting the cross section data of $\rho^0$, $\omega$, and $\phi$ photoproduction [42], the parameters of the model have been determined to be

$$\begin{aligned} \mu_0 &= 1.1 \text{ GeV}^2, \\ \beta_{u/d} &= 2.07 \text{ GeV}^{-1}, \\ \beta_s &= 1.386 \text{ GeV}^{-1}, \\ \alpha_0 &= 1.08, \\ \alpha_P' &= 1/s_0 = 0.25 \text{ GeV}^{-2}. \end{aligned} \tag{19}$$

For heavy quark systems, it was found [36] that, with the same values of $\mu_0^2$, $\beta_{u/d}$, and $\alpha_P'$, the $J/\psi$ and $\Upsilon(1s)$ photoproduction data could be fit by choosing $\beta_c = 0.323$ GeV$^{-1}$ and $\beta_b = 0.452$ GeV$^{-1}$ with $\alpha_0 = 1.25$. The intercept parameter $\alpha_0$ of the Pomeron for heavy quarks ($c$ and $b$) production is rather different from that for the light quarks ($u$, $d$, $s$). More rigorous studies are needed to understand this observation, which is, however, beyond the scope of this work.

Shown in Fig. 4 are the fits to the total cross-section data of $\rho^0$, $\phi$, $J/\psi$, and $\Upsilon(1s)$ mesons. The experimental data for $\phi$, $J/\psi$, and $\Upsilon(1s)$ production processes are found to be well described by the Pomeron-exchange model at high energies. On the other hand, the $\rho^0$ and $\omega$ production data at low energies clearly need other mechanisms such as meson-exchange mechanisms [41,45].

### B. Meson exchange

The electromagnetic-interaction Lagrangians for the pseudoscalar, scalar, and $f_1(1285)$ axial-vector-meson exchanges

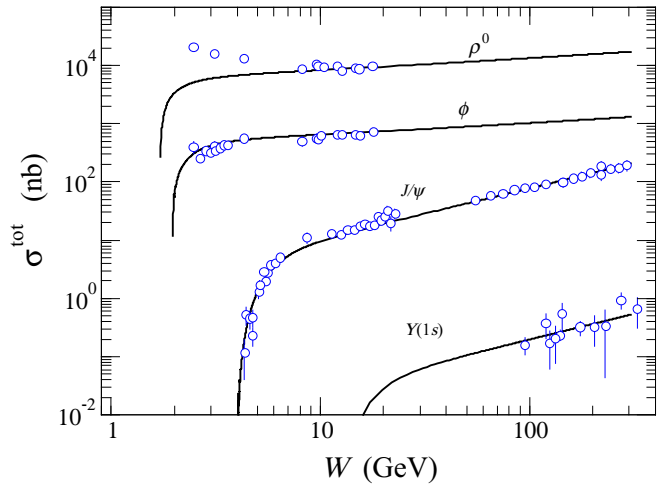


FIG. 4. Total cross sections for photoproduction of $\rho^0$, $\phi$, $J/\psi$, and $\Upsilon(1s)$ on proton targets. The data are from Ref. [46].

are given as

$$\begin{aligned} \mathcal{L}_{\gamma\Phi\phi} &= \frac{e g_{\gamma\Phi\phi}}{M_\phi}\epsilon^{\mu\nu\alpha\beta}\partial_\mu A_\nu \partial_\alpha \phi_\beta \Phi, \\ \mathcal{L}_{\gamma S\phi} &= \frac{e g_{\gamma S\phi}}{M_\phi} F^{\mu\nu}\phi_{\mu\nu} S, \\ \mathcal{L}_{\gamma f_1\phi} &= g_{\gamma f_1\phi}\epsilon^{\mu\nu\alpha\beta}\partial_\mu A_\nu \partial^\lambda \partial_\lambda \phi_\alpha f_{1\beta}, \end{aligned} \tag{20}$$

where $\Phi$, $S$, and $f_1$ stand for the fields for the pseudoscalar, scalar, and $f_1(1285)$ mesons, respectively. In the present work, we consider $\Phi = \pi^0(135)$, $\eta(548)$ and $S = a_0(980)$, $f_0(980)$. The photon and $\phi$-meson field strength tensors are $F^{\mu\nu} = \partial^\mu A^\nu - \partial^\nu A^\mu$ and $\phi^{\mu\nu} = \partial^\mu \phi^\nu - \partial^\nu \phi^\mu$, respectively.

The coupling constants are determined by the radiative decay widths of $\phi \to \Phi\gamma$, $\phi \to S\gamma$, and $f_1 \to \phi\gamma$, which are

$$\begin{aligned} \Gamma_{\phi\to\Phi\gamma} &= \frac{e^2}{12\pi}\frac{q_\gamma^3}{M_\phi^2} g_{\gamma\Phi\phi}^2, \\ \Gamma_{\phi\to S\gamma} &= \frac{e^2}{3\pi}\frac{q_\gamma^3}{M_\phi^2} g_{\gamma S\phi}^2, \\ \Gamma_{f_1\to\phi\gamma} &= \frac{k_\gamma^3}{12\pi}\frac{M_\phi^2}{M_{f_1}^2}\left(M_{f_1}^2 + M_\phi^2\right) g_{\gamma f_1\phi}^2, \end{aligned} \tag{21}$$

where

$$\begin{aligned} q_\gamma &= \left(M_\phi^2 - M_{\Phi,S}^2\right)/(2M_\phi), \\ k_\gamma &= \left(M_{f_1}^2 - M_\phi^2\right)\big/\left(2M_{f_1}\right). \end{aligned} \tag{22}$$

Using the branching ratio data of the radiative decays [43],

$$\begin{aligned} \text{Br}(\phi\to\pi\gamma) &= 1.32\times10^{-3}, \\ \text{Br}(\phi\to\eta\gamma) &= 1.303\times10^{-2}, \\ \text{Br}(\phi \to a_0\gamma) &= 7.6 \times 10^{-5}, \\ \text{Br}(\phi \to f_0\gamma) &= 3.22 \times 10^{-4}, \\ \text{Br}(f_1 \to \phi\gamma) &= 7.5\times10^{-4}, \end{aligned} \tag{23}$$

$f_V = 4.94$, 17.06, 13.38, 11.18, and 39.68 for $\rho^0$, $\omega$, $\phi$, $J/\psi$, and $\Upsilon(1s)$ mesons, respectively, using the values quoted by the Particle Data Group [43].

we obtain

$$\begin{aligned} g_{\gamma\pi\phi} &= -0.14, \\ g_{\gamma\eta\phi} &= -0.71, \\ g_{\gamma a_0\phi} &= -0.77, \\ g_{\gamma f_0\phi} &= -2.44, \\ g_{\gamma f_1\phi} &= 0.17\ \text{GeV}^{-2}, \end{aligned} \tag{24}$$

by following Ref. [27] for the phases of the coupling constants.

The strong-interaction Lagrangians for describing meson exchanges are

$$\begin{aligned} \mathscr{L}_{\Phi NN} &= -ig_{\Phi NN}\bar{N}P\gamma_5 N, \\ \mathscr{L}_{SNN} &= -g_{SNN}\bar{N}SN, \\ \mathscr{L}_{f_1NN} &= -g_{f_1NN}\bar{N}\Big(\gamma_\mu - i\frac{\kappa_{f_1NN}}{2M_N}\gamma_\nu\gamma_\mu\partial^\nu\Big)f_1^\mu\gamma_5 N. \end{aligned} \tag{25}$$

The strong-coupling constants are obtained by using the Nijmegen potential as [47,48]

$$\begin{aligned} g_{\pi NN} &= 13.0, \quad g_{\eta NN} = 6.34, \\ g_{a_0NN} &= 4.95, \quad g_{f_0NN} = -0.51. \end{aligned} \tag{26}$$

Following Refs. [49,50], the coupling of the $f_1$ meson is taken as

$$|g_{f_1NN}| = 2.5. \tag{27}$$

We neglect the $f_1$ tensor term by setting $\kappa_{f_1NN} = 0$ in the present calculation for simplicity.

The invariant amplitudes for the pseudoscalar, scalar, and axial-vector-meson exchanges read

$$\begin{aligned} \mathcal{M}_\Phi^{\mu\nu} &= \frac{ie}{M_\phi}\frac{g_{\gamma\Phi\phi}g_{\Phi NN}}{t-M_\Phi^2}\epsilon^{\mu\nu\alpha\beta}q_\alpha k_\beta\gamma_5, \\ \mathcal{M}_S^{\mu\nu} &= \frac{e}{M_\phi}\frac{2g_{\gamma S\phi}g_{SNN}}{t-M_S^2+i\Gamma_S M_S}(q\cdot k g^{\mu\nu} - q^\nu k^\mu), \\ \mathcal{M}_{f_1}^{\mu\nu} &= iM_\phi^2 g_{\gamma f_1\phi}g_{f_1NN}\epsilon^{\mu\nu\alpha\beta}\left(-g_{\alpha\lambda} + \frac{q_{t\alpha}q_{t\lambda}}{M_{f_1}^2}\right) \\ &\quad\times\left(\gamma^\lambda + \frac{\kappa_{f_1NN}}{2M_N}\gamma^\sigma\gamma^\lambda q_{t\sigma}\right)\gamma_5 q_\beta P_{f_1}(t), \end{aligned} \tag{28}$$

where $q_t = p_i - p_f$ and $M_H$ is the mass of hadron $H$ with $M_{a_0} = 980$ MeV and $M_{f_0} = 990$ MeV with $\Gamma_{a_0} \approx \Gamma_{f_0} \approx 75$ MeV [43].

To preserve the unitarity condition, we use the Regge prescription for $\mathcal{M}_{f_1}$. The Regge propagator of the $f_1$ meson is given by

$$P_{f_1}(t) = \left(\frac{s}{s_{f_1}}\right)^{\alpha_{f_1}(t)-1}\frac{\pi\alpha'_{f_1}}{\sin\big[\pi\alpha_{f_1}(t)\big]}\frac{1}{\Gamma\big[\alpha_{f_1}(t)\big]}D_{f_1}(t), \tag{29}$$

where $s_{f_1} = 1$ GeV$^2$ and the $f_1$ Regge trajectory is $\alpha_{f_1} = 0.95 + 0.028t$ [50]. The signature factor in Eq. (29) is of the form [50]

$$D_{f_1}(t) = \frac{\exp\big[-i\pi\alpha_{f_1}(t)\big]-1}{2}. \tag{30}$$

Each vertex in these amplitudes of meson exchanges is dressed by the form factor in the form of

$$F_M(t) = \frac{\Lambda_M^4}{\Lambda_M^4 + \big(t-M_M^2\big)^2}. \tag{31}$$

The cutoff parameters are determined as $(\Lambda_\Phi,\ \Lambda_S,\ \Lambda_{f_1}) = (0.25,\ 1.22,\ 1.50)$ GeV.

### C. Direct $\phi$ meson radiations

The effective Lagrangians for the direct $\phi$ radiations read

$$\begin{aligned} \mathscr{L}_{\gamma NN} &= -e\bar{N}\left[\gamma_\mu - \frac{\kappa_N}{2M_N}\sigma_{\mu\nu}\partial^\nu\right]NA^\mu, \\ \mathscr{L}_{\phi NN} &= -g_{\phi NN}\bar{N}\left[\gamma_\mu - \frac{\kappa_{\phi NN}}{2M_N}\sigma_{\mu\nu}\partial^\nu\right]N\phi^\mu, \end{aligned} \tag{32}$$

where $\kappa_p = 1.79$. The $\phi NN$ coupling constant is determined by using the Nijmegen potential as [47,48][2]

$$g_{\phi NN} = -1.47, \quad \kappa_{\phi NN} = -1.65. \tag{33}$$

The $\phi$-radiation amplitudes are then obtained as

$$\begin{aligned} \mathcal{M}_{\phi,\text{rad},s}^{\mu\nu} &= \frac{eg_{\phi NN}}{s-M_N^2}\left(\gamma^\nu - i\frac{\kappa_{\phi NN}}{2M_N}\sigma^{\nu\alpha}k_\alpha\right) \\ &\quad\times(\not{q}_s + M_N)\left(\gamma^\mu + i\frac{\kappa_N}{2M_N}\sigma^{\mu\beta}q_\beta\right), \\ \mathcal{M}_{\phi,\text{rad},u}^{\mu\nu} &= \frac{eg_{\phi NN}}{u-M_N^2}\left(\gamma^\mu + i\frac{\kappa_N}{2M_N}\sigma^{\mu\alpha}q_\alpha\right) \\ &\quad\times(\not{q}_u + M_N)\left(\gamma^\nu - i\frac{\kappa_{\phi NN}}{2M_N}\sigma^{\nu\beta}k_\beta\right), \end{aligned} \tag{34}$$

for $s$ and $u$ channels, respectively. The four-momenta of the intermediate particles are defined as $q_s = q + p_i$ and $q_u = p_f - q$.

For the form factor of the $\gamma NN$ vertex, we consider the form of Eq. (31) to have

$$F_N(x) = \frac{\Lambda_N^4}{\Lambda_N^4 + \big(x-M_N^2\big)^2}, \tag{35}$$

for $x = (s, u)$. Following Ref. [52], we take the common form factor as

$$F_c(s,u) = [F_N(s) + F_N(u) - F_N(s)F_N(u)]^2. \tag{36}$$

For the $\phi NN$ vertex, we use

$$F_N(\mathbf{k}) = \left(\frac{\Lambda_N^2}{\Lambda_N^2 + \mathbf{k}^2}\right)^2, \tag{37}$$

following the ANL-Osaka formulation, where $\mathbf{k}$ is the three-momentum of the produced $\phi$ meson. This choice is to ensure the convergence of the integration in calculating the FSI effect.

[2]We note that smaller values of the $\phi NN$ coupling strength are obtained by kaon loop calculations in Ref. [51].

The final form of the $\phi$-radiation amplitude then becomes

$$\mathcal{M}_{\phi,\mathrm{rad}} = (\mathcal{M}_{\phi,\mathrm{rad},s} + \mathcal{M}_{\phi,\mathrm{rad},u})F_c(s,u)F_N(\mathbf{k}). \tag{38}$$

Similar amplitudes are needed to estimate the FSI effects through the $\phi p \to \phi p$ reaction, as depicted in Figs. 2(b) and 2(c). For considering the FSI effects, we use the same form factor as given in Eqs. (36) and (37). However, the differential cross-section data of $\phi$ photoproduction in the far backward direction, $\cos\theta \leqslant -0.8$, are very limited [53]. Since the $N$-exchange contribution rises at very large scattering angles [27], the paucity of the data does not allow us to precisely pin down the contribution from the $N$ exchange diagrams. In the present work, therefore, we fix its strength by $\Lambda_N = 0.98$ GeV.

### D. $N^*$ excitation terms

The calculation of the $N^*$ amplitude in Eq. (9) requires a full coupled-channels calculation for the evaluation of the dressed vertex $\bar{\Gamma}_{N^*,\phi N}$ and the self-energy $\Sigma_{N^*}(E)$. The details can be found, for example, in Refs. [22,23]. In this exploratory study, however, we make a simplification by assuming $M_{N^*} - \Sigma_{N^*}(E) \sim M_{N^*} + \frac{i}{2}\Gamma^{\mathrm{tot}}(E)$, so that the resulting form is reduced to the usual Breit-Wigner form. In the c.m. system, the amplitude of $\gamma(\mathbf{q},\lambda_\gamma) + N(-\mathbf{q},\lambda_N) \to N^*(J,M_J) \to \phi(\mathbf{k},m_\phi) + N(-\mathbf{k},m_s')$ can then be written as [22]

$$\begin{aligned}&\langle \mathbf{k}, m_\phi m_s' | T^J | \mathbf{q}, \lambda_\gamma \lambda_N \rangle \\ &= \sum_{M_J} \langle \mathbf{k}, m_\phi m_s' | \bar{\Gamma}_{N^*,\phi N} | J M_J \rangle \frac{1}{W - M_{N^*} + \frac{i}{2}\Gamma^{\mathrm{tot}}(W)} \\ &\times \langle J M_J | \Gamma^\dagger_{N^*,\gamma N} | \mathbf{q}, \lambda_\gamma \lambda_N \rangle ,\end{aligned} \tag{39}$$

where $\lambda_\gamma$ and $\lambda_N$ are the helicities of the photon and the incoming nucleon, respectively, and $m_\phi$ and $m_s'$ are spin projections of the $\phi$ and recoiled nucleon. The spin and its projection of the intermediate $N^*$ are denoted by $J$ and $M_J$, respectively. The matrix element of the $\gamma N \to N^*$ transition is

$$\begin{aligned}&\langle J M_J | \Gamma^\dagger_{N^*,\gamma N} | \mathbf{q}, \lambda_\gamma \lambda_N \rangle \\ &= \delta_{\lambda,(\lambda_\gamma - \lambda_N)} \frac{1}{(2\pi)^{3/2}} \sqrt{\frac{M_N q_{N^*}}{E_N q}} A_\lambda D^J_{\lambda,M_J}(\phi_q,\theta_q,-\phi_q),\end{aligned} \tag{40}$$

where $A_\lambda$ is the helicity amplitude of the $\gamma N \to N^*$ excitation, $q_{N^*}$ and $q$ are determined by $M_R = q_{N^*} + E_N(q_{N^*})$ and $W = q + E_N(q)$, respectively, and

$$D^J_{\lambda,M_J}(\phi_q,\theta_q,-\phi_q) = e^{i(\lambda - M_J)\phi} d^J_{\lambda,M_J}(\theta_q). \tag{41}$$

Here $d^J_{\lambda,M_J}(\theta_q)$ is the Wigner $d$ function.

The matrix element of the $N^* \to \phi N$ transition is

$$\begin{aligned}&\langle \mathbf{k}, m_\phi m_s' | \bar{\Gamma}_{N^*,\phi N} | J M_J \rangle \\ &= \sum_{LS} \sum_{M_L M_S} \langle J M_J | L S M_L M_S \rangle \left\langle S M_S \middle| 1\tfrac{1}{2} m_\phi m_s \right\rangle Y_{LM_L}(\hat{\mathbf{k}}) \\ &\times \frac{1}{(2\pi)^{3/2}} \frac{1}{\sqrt{2E_\phi(k)}} \sqrt{\frac{M_N}{E_N(k)}} \sqrt{\frac{8\pi^2 M_{N^*}}{M_N k}} G^J_{LS} \left(\frac{k}{k_{N^*}}\right)^L ,\end{aligned} \tag{42}$$

where $k$ and $k_{N^*}$ are determined by $W = E_\phi(k) + E_N(k)$ and $M_{N^*} = E_\phi(k_{N^*}) + E_N(k_{N^*})$. The partial decay widths are defined by

$$\begin{aligned}d\Gamma_{N^*,\gamma N} &= (2\pi)\delta(M_{N^*} - E_N(q) - q) \\ &\times \frac{1}{2J+1} \sum_{M_J} \sum_{\lambda_\gamma \lambda_N} |\langle \mathbf{q}, \lambda_\gamma \lambda_N | \bar{\Gamma}^\dagger_{N^*,\gamma N} | J M_J \rangle|^2 \\ &\times q^2 dq d\Omega_q , \\ d\Gamma_{N^*,\phi N} &= (2\pi)\delta(M_{N^*} - E_\phi(k) - E_N(k)) \\ &\times \frac{1}{2J+1} \sum_{M_J} \sum_{m_\phi m_N} |\langle \mathbf{k}, m_\phi m_s' | \bar{\Gamma}_{N^*,\phi N} | J M_J \rangle|^2 \\ &\times k^2 dk d\Omega_k .\end{aligned} \tag{43}$$

Integrating over the phase space, the parameters $A_\lambda$ and $G^J_{LS}$ are found to be related to the partial decay widths as

$$\Gamma_{N^*,\gamma N} = \frac{q^2_{N^*}}{4\pi} \frac{M_N}{M_{N^*}} \frac{8}{2J+1} (|A_{1/2}|^2 + |A_{3/2}|^2), \tag{44}$$

$$\Gamma_{N^*,\phi N} = \sum_{LS} \left| G^J_{LS} \right|^2 . \tag{45}$$

We follow the model of Ref. [28] for the $\gamma N \to N^* \to \phi N$ cross sections to include $N^*(2000, 5/2^+)$ and $N^*(2300, 1/2^+)$. The resonance parameters are taken similarly from Ref. [28]. For $N^*(2000, 5/2^+)$, we use

$$\begin{aligned}\Gamma^{\mathrm{tot}} &= 200 \text{ MeV}, \\ A_{1/2} &= 0.031 \text{ GeV}^{-1/2}, \\ A_{3/2} &= -0.43 \text{ GeV}^{-1/2}, \\ G_{LS} &= G_{2\frac{1}{2}} = 0.547 \text{ MeV},\end{aligned} \tag{46}$$

and the parameters of $N^*(2300, 1/2^+)$ are

$$\begin{aligned}\Gamma^{\mathrm{tot}} &= 300 \text{ MeV}, \\ A_{1/2} &= 0.031 \text{ GeV}^{-1/2}, \\ A_{1/2} &= 0.0, \\ G_{LS} &= G_{0\frac{1}{2}} = 2.80 \text{ MeV}.\end{aligned} \tag{47}$$

We also employ the Gaussian form factor [28]

$$F_{N^*}(s) = \exp\left[\frac{-(s - M^2_{N^*})^2}{\Lambda^4_{N^*}}\right], \tag{48}$$

with $\Lambda_{N^*} = 1.0$ GeV. Our results are shown in Fig. 5, which is similar to Fig. 3(b) of Ref. [28].

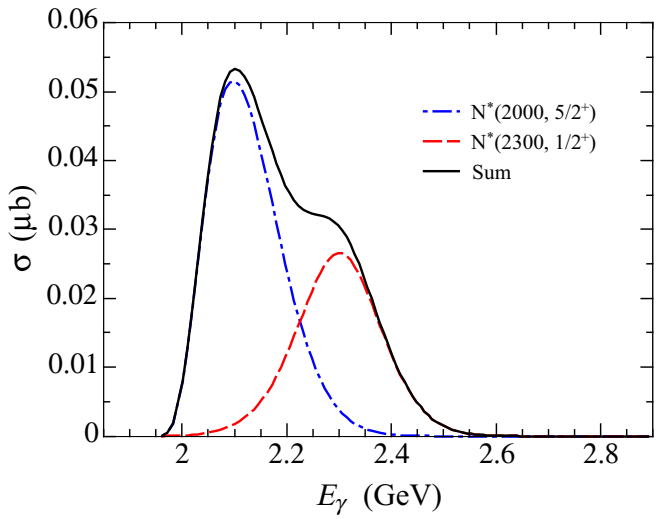


FIG. 5. $N^*$ contributions to the total cross section of $\gamma p \to \phi p$.

## IV. THE FINAL-STATE INTERACTION AMPLITUDE

The amplitude for final-state interactions is defined in Eqs. (4)–(8). In the present work, we focus on examining the relative importance among the gluon exchange term $v^{\rm Gluon}_{\phi N,\phi N}$, direct $\phi N$ coupling term $v^{\rm Direct}_{\phi N,\phi N}$, and box-diagram term $v^{\rm Box}_{\phi N,\phi N}$. This can be done by keeping the leading term in Eq. (6) with taking the approximation that $t_{\phi N,\phi N}(E) \sim V_{\phi N,\phi N}(E)$ in evaluating the FSI amplitude in Eq. (4). In the c.m. frame, the amplitude $T^{\rm FSI}_{\phi N,\gamma N}(E)$ of Eq. (4) for the reaction of $\gamma(\mathbf{q}) + N(-\mathbf{q}) \to \phi(\mathbf{k}) + N(-\mathbf{k})$ can then be obtained as

$$\langle \mathbf{k}|T^{\rm FSI}_{\phi N,\gamma N}(E)|\mathbf{q}\rangle = \int d\mathbf{k}'\, \langle \mathbf{k}|V_{\phi N,\phi N}(E)|\mathbf{k}'\rangle \times \frac{1}{E - E_\phi(k') - E_N(k') + i\epsilon}\, \langle \mathbf{k}'|B_{\phi N,\gamma N}(E)|\mathbf{q}\rangle\,. \quad (49)$$

The main task is then to evaluate the matrix elements of the potential of $V_{\phi N,\phi N}(E)$ for $\phi(k') + N(p') \to \phi(k) + N(p)$, which can be written as

$$\langle k\lambda_\phi; pm_s|V_{\phi N,\phi N}|k'\lambda'_\phi; p'm'_s\rangle = \frac{1}{(2\pi)^3}\sqrt{\frac{M_N^2}{4E_\phi(\mathbf{k})E_N(\mathbf{p})E_\phi(\mathbf{k}')E_N(\mathbf{p}')}} \times \mathcal{V}(k\lambda_\phi, pm_s; k'\lambda'_\phi, p'm'_s), \quad (50)$$

where $E_\phi$ and $E_N$ are the energies of the $\phi$ meson and the nucleon, respectively, and

$$\mathcal{V} = \mathcal{V}_{\rm Gluon} + \mathcal{V}_{\rm Direct} + \sum_{MB=K\Lambda,K\Sigma,\pi N,\rho N} \mathcal{V}_{MB}(E). \quad (51)$$

Here, $\mathcal{V}_{\rm Gluon}$ [Fig. 2(a)] and $\mathcal{V}_{\rm Direct}$ [Figs. 2(b) and 2(c)] are from the gluon-exchange interaction and the direct $\phi N$ coupling term, respectively, and $\mathcal{V}_{MB}(E)$ [Figs. 2(d)–(f)] includes the box-diagram mechanisms defined by Eq. (8). In the following sections, we elaborate on calculating these $\phi N$ potentials from the interaction Lagrangians by using the unitary transformation method of the ANL-Osaka formulation [23].

### A. Gluon-exchange interaction

Because of the OZI rule, the $\phi N$ interaction is expected to be governed by gluon exchanges. However, since there exists no LQCD calculations for the $\phi N$ potential, we use the form suggested by the recent analysis of Ref. [54] for the charmonium-nucleon potential. It was found that that the calculated charmonium-nucleon potential is approximately of the Yukawa form which has also been assumed in phenomenological studies [55] of the $\phi N$ interactions. We, therefore, take the form of

$$\mathcal{V}_{\rm gluon} = -v_0 \frac{e^{-\alpha r}}{r}. \quad (52)$$

For the charmonium-nucleon system, the LQCD data of Ref. [54] can be approximated by the above form with $v_0 = 0.06$ and $\alpha = 0.3$ GeV. Since the $\phi N$ potential is expected to have different range and the strength, we consider the range of parameters as $0.1 < v_0 < 1.0$ and $0.3 < \alpha < 0.6$ GeV. As will be discussed in Sec. VI, the best fit to the $\phi$ photoproduction data was obtained by setting $v_0 = 0.2$ and $\alpha = 0.5$ GeV.

The potential of Eq. (52) can be obtained by taking the nonrelativistic limit of the scalar-meson exchange amplitude calculated from the Lagrangian,

$$\mathcal{L}_\sigma = V_0(\bar\psi_N \psi_N \Phi_\sigma + \phi^\mu \phi_\mu \Phi_\sigma), \quad (53)$$

where $\Phi_\sigma$ is a scalar field with mass $\alpha$ in Eq. (52). By using the unitary transformation method used by the ANL-Osaka formulation, the scalar-meson exchange matrix element derived from Eq. (53) is in the form

$$\mathcal{V}_{\rm gluon}(k\lambda_\phi, pm_s; k'\lambda'_\phi, p'm'_s) = \frac{V_0}{(p-p')^2 - \alpha^2} \times [\bar u_N(p, m_s)u_N(p', m'_s)][\epsilon^*_\mu(k, \lambda_\phi)\epsilon^\mu(k', \lambda'_\phi)], \quad (54)$$

where $V_0 = -8v_0\pi M_\phi$ and $(p - p') = (E_N(p) - E_N(p'),\ \mathbf{p} - \mathbf{p}')$. We will use this form in our calculations.

### B. Direct $\phi N$ coupling term

The form of the direct $\phi N$ coupling amplitudes is the same as given in Eqs. (34) and (38) after the replacement of $e$ by $g_{\phi NN}$ and $\kappa_N$ by $\kappa_{\phi NN}$. We also use the same form of the form factors as given in Eqs. (35)–(37) and the same cutoff parameter, i.e., $\Lambda_N = 0.98$ GeV.

### C. Box-diagram mechanisms

To calculate the box diagrams depicted in Figs. 2(d)–2(f), the transition potentials for $\phi N \to K\Lambda$, $K\Sigma$, $\pi N$, $\rho N$ are needed, which can be constructed by the interaction Lagrangians given below. The $\phi N \to KY (Y = \Lambda, \Sigma)$ processes

are described by

$$\mathscr{L}_{\phi KK} = ig_{\phi KK}(K^-\partial_\mu K^+ - \partial_\mu K^- K^+)\phi^\mu, \tag{55}$$

$$\mathscr{L}_{KNY} = -\frac{f_{KNY}}{M_K}\bar{Y}\gamma_\mu\gamma_5 N\partial^\mu K + \text{H.c.}, \tag{56}$$

where the coupling constant $g_{\phi KK} = 4.48$ is determined from the experimental data for the decay width, $\Gamma_{\phi\to K^+K^-} = 2.09$ MeV, where

$$\Gamma_{\phi\to K^+K^-} = \frac{g^2_{\phi KK}p^3_K}{6\pi M^2_\phi}, \tag{57}$$

with $p_K = (M^2_\phi - 4M^2_K)^{1/2}/2$.

For the $\phi N \to \pi N$ and $\phi N \to \rho N$ processes, we use

$$\mathscr{L}_{\phi\rho\pi} = -\frac{g_{\phi\rho\pi}}{M_\phi}\epsilon^{\mu\nu\alpha\beta}(\partial_\mu \boldsymbol{\rho}_\nu)\cdot(\partial_\alpha\boldsymbol{\pi})\phi_\beta, \tag{58}$$

$$\mathscr{L}_{\rho NN} = g_{\rho NN}\bar{N}\left(\boldsymbol{\rho}_\mu\gamma^\mu - \frac{\kappa_{\rho NN}}{2M_N}\sigma^{\mu\nu}\partial_\nu\boldsymbol{\rho}_\mu\right)\cdot\boldsymbol{\tau}N, \tag{59}$$

$$\mathscr{L}_{\pi NN} = -\frac{f_{\pi NN}}{M_\pi}\bar{N}\gamma_\mu\gamma_5\boldsymbol{\tau}\cdot(\partial^\mu\boldsymbol{\pi})N, \tag{60}$$

where $g_{\phi\rho\pi} = 1.22$ is determined by the decay width of $\phi \to \rho\pi$. The $\rho NN$ coupling constant is determined by using the Nijmegen potential [47,48],

$$g_{\rho NN} = 2.97, \quad \kappa_{\rho NN} = 4.22. \tag{61}$$

The couplings of pseudoscalar mesons and baryons are determined by the SU(3) flavor symmetry relations,

$$\frac{f_{KN\Lambda}}{M_K} = \frac{-3+2\alpha}{\sqrt{3}}\frac{f_{\pi NN}}{M_\pi},$$
$$\frac{f_{KN\Sigma}}{M_K} = (-1+2\alpha)\frac{f_{\pi NN}}{M_\pi}. \tag{62}$$

With $\alpha = 0.635$ and $f_{\pi NN}/\sqrt{4\pi} = \sqrt{0.08}$, we get $f_{KN\Lambda} = -3.46$ and $f_{KN\Sigma} = 0.92$.

For the reaction of $\phi(k') + N(p') \to M(k) + B(p)$, the amplitudes of $K$, $\rho$, and $\pi$ exchanges derived by using the unitary transformation method from the above Lagrangians can be expressed as

$$I_{MB,\phi N}(k, pm_s; k'\lambda'_\phi, p'm'_s)$$
$$= \bar{u}_B(p, m_s)I^\mu_{MB,\phi N}u_N(p', m'_s)\epsilon_\mu(k', \lambda'_\phi), \tag{63}$$

where

$$I^\mu_{KY,\phi N} = i\frac{g_{\phi KK}f_{KNY}}{M_K}\frac{1}{q^2 - M^2_K}\not{q}\gamma_5(k-q)^\mu, \tag{64}$$

$$I^\mu_{\pi N,\phi N} = -\frac{g_{\phi\rho\pi}g_{\rho NN}}{M_\phi}\frac{1}{q^2 - M^2_\rho}\epsilon^{\mu\nu\alpha\beta}k_\nu q_\alpha$$
$$\times\left[\gamma_\beta - \frac{\kappa_{\rho NN}}{4M_N}(\gamma_\beta\not{q} - \not{q}\gamma_\beta)\right], \tag{65}$$

$$I^\mu_{\rho N,\phi N} = \sum_{\lambda_\rho} -i\frac{g_{\phi\rho\pi}}{M_\phi}\frac{f_{\pi NN}}{M_\pi}\frac{1}{q^2 - M^2_\pi}\epsilon^{\mu\nu\alpha\beta}k_\nu q_\alpha$$
$$\times\epsilon^*_\beta(k, \lambda_\rho)\not{q}\gamma_5. \tag{66}$$

Here, $q = p' - p = (E_N(p') - E_B(p),\ \mathbf{p}' - \mathbf{p})$, $B = Y$ or $N$, and the polarization vector $\epsilon_\beta(k, \lambda_\rho)$ of the $\rho$ meson with momentum $k$ and helicity $\lambda_\rho$ is introduced.

We consider the following form factor for the $\phi M$ vertex:

$$F_{\text{Box}}(\mathbf{k}_{MB}) = \left(\frac{\Lambda^2_{MB}}{\Lambda^2_{MB} + \mathbf{k}^2_{MB}}\right)^2, \tag{67}$$

and

$$F'_{\text{Box}}(\mathbf{k}'_{MB}) = \left(\frac{\Lambda'^2_{MB}}{\Lambda'^2_{MB} + \mathbf{k}'^2_{MB}}\right)^2, \tag{68}$$

for the $NB$ vertex, where

$$\mathbf{k}^2_{MB} = \sum_{i=1,3}\left(\frac{\mathbf{k}_i q_0 - \mathbf{q}_i k_0}{q_0 + k_0}\right)^2,$$
$$\mathbf{k}'^2_{MB} = \mathbf{q}^2 = (\mathbf{p}' - \mathbf{p})^2. \tag{69}$$

We choose the cutoff parameters to be 650–1200 MeV which are in the range of the meson-exchange amplitude determined in the ANL-Osaka analysis of the $\pi N$ and $\gamma N$ reactions. Explicitly, their values are chosen as

$$\Lambda_{K\Lambda,K\Sigma,\pi N,\rho N} = 860\ \text{MeV}, \quad \Lambda'_{K\Lambda,K\Sigma} = 1200\ \text{MeV},$$
$$\Lambda'_{\pi N} = 920\ \text{MeV}, \quad \Lambda'_{\rho N} = 656\ \text{MeV}. \tag{70}$$

In the c.m. frame, in which the scattering cross sections are evaluated, the matrix element of the box-diagram mechbrk anism is calculated from

$$\mathcal{V}_{\text{MB}}(k\lambda_\phi, pm_s; k'\lambda'_\phi, p'm'_s)$$
$$= \sum_{MB=K\Lambda,\pi N,\rho N}\int d\boldsymbol{\kappa} I_{\phi N,MB}(k\lambda_\phi, pm_s; p_M, p_B m_B)$$
$$\times\frac{1}{(2\pi)^3}\frac{1}{2E_M(\boldsymbol{\kappa})}\frac{M_B}{E_B(\boldsymbol{\kappa})}\frac{1}{W - E_M(\boldsymbol{\kappa}) - E_B(\boldsymbol{\kappa}) + i\epsilon}$$
$$\times I_{MB,\phi N}(p_M, p_B m_B; k'\lambda'_\phi, p'm'_s), \tag{71}$$

where $\mathbf{p} = -\mathbf{k}$, $\mathbf{p}' = -\mathbf{k}'$, $p_M = (E_M, \boldsymbol{\kappa})$, and $p_B = (E_B, -\boldsymbol{\kappa})$. The matrix elements $I_{\phi N,MB}$ and $I_{MB,\phi N}$ in the above equation are constructed by using the unitary-transformation method of the ANL-Osaka approach and are free of singularities. The only singularities in the integrations are from the $MB$ propagator. In this work, both the singular and principal parts are calculated by using the well-established numerical method.

## V. FORMULATION FOR $A(\gamma, \phi)A$ REACTION

The differential cross section of coherent photoproduction of a vector meson ($V$) on a nuclear target ($A$) with $A$ nucleons, $\gamma(q) + A(P_i) \to V(k) + A(P_f)$, are obtained as

$$\frac{d\sigma}{dt} = \frac{\pi}{|\mathbf{q}||\mathbf{k}|}\frac{d\sigma}{d\Omega_{\text{Lab}}}, \tag{72}$$

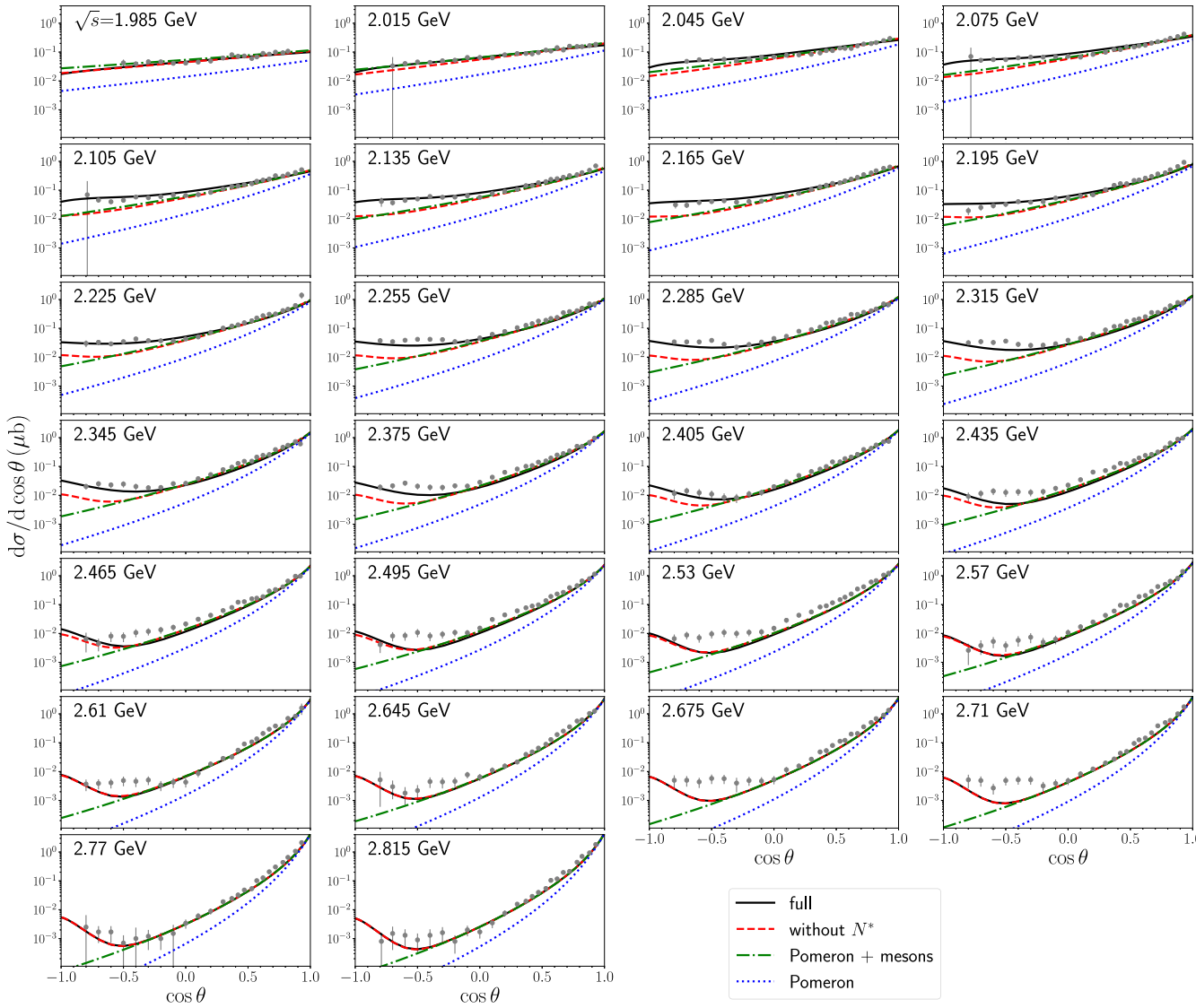


FIG. 6. Differential cross sections $d\sigma/d\cos\theta$ of the $\gamma p \to \phi p$ reaction without FSI as functions of $\cos\theta$ for energies $\sqrt{s} = W =$ (1.985–2.815) GeV. The blue dotted lines are from the calculations including Pomeron exchange only. The green dot-dashed lines show the sum of the Pomeron and meson exchange mechanisms. The black solid lines and the red dashed lines represent the full contribution with and without $N^*$, respectively, which are almost identical at $\sqrt{s} \geqslant 2.57$ GeV. The experimental data are from the CLAS Collaboration [53].

where the differential cross section in the laboratory (Lab) frame ($\mathbf{P}_i = 0$) is

$$\frac{d\sigma}{d\Omega_{\rm Lab}} = \frac{(2\pi)^4 |\mathbf{k}|^2 E_V(\mathbf{k}) E_A(\mathbf{q}-\mathbf{k})}{|E_A(\mathbf{q}-\mathbf{k})|\mathbf{k}| + E_V(\mathbf{k})(|\mathbf{k}| - |\boldsymbol{q}|\cos\theta_{\rm Lab})|} \times \frac{1}{2(2J+1)} \times \left| \left\langle k\lambda_V, \Phi_{P_f M_{J_f}} \middle| T(E) \middle| q\lambda_\gamma, P_i \Phi_{P_i, M_{J_i}} \right\rangle \right|^2, \quad (73)$$

where $\cos\theta_{\rm Lab} = \hat{\mathbf{q}} \cdot \hat{\mathbf{k}}$. Within the distorted-wave impulse approximation of multiple-scattering theory [34], the scattering $T$ matrix defined by the Hamiltonian of Eq. (2) can be written as

$$T(E) = T^{\rm IMP}(E) + T^{\rm FSI}(E), \quad (74)$$

where

$$T^{\rm IMP} = \sum_{i=1,A} \left[ B_{\phi N_i, \gamma N_i} + T^{N^*}_{\phi N_i, \gamma N_i} \right],$$

$$T^{\rm FSI}(E) = T_{\phi A, \phi A}(E) \frac{1}{E - H_0} T^{\rm IMP}. \quad (75)$$

The impulse term $T^{\rm IMP}$ is the term that the $\phi$ meson is produced from a single nucleon in the nucleus, and $T^{\rm FSI}$ is the effect due to the scattering of the outgoing $\phi$ with the recoiled nucleus. The $\phi A \to \phi A$ scattering $T$ matrix is defined

by

$$T_{\phi A,\phi A}(E) = U_{\phi A,\phi A}(E) + U_{\phi A,\phi A}(E)\frac{1}{E - H_0 + i\epsilon}T_{\phi A,\phi A}(E), \quad (76)$$

where $U_{\phi A,\phi A}(E)$ is the $\phi A$ potential.

Within multiple-scattering theory [34], one can define the $\phi A$ potential in terms of the $\phi N$ scattering amplitude. To first order, we have

$$U_{\phi A,\phi A}(E) = \sum_{i=1,A} t_{\phi N_i,\phi N_i}(\omega), \quad (77)$$

where $t_{\phi N_i,\phi N_i}(\omega)$ was defined in Eq. (6). We take the widely used factorization approximation [34] to evaluate the matrix element of $U_{\phi A,\phi A}(E)$. In the c.m. frame, for the reaction of $\phi(\boldsymbol{\kappa}) + A(-\boldsymbol{\kappa}) \to \phi(\boldsymbol{\kappa}') + A(-\boldsymbol{\kappa}')$, we have

$$U_{\phi A,\phi A}(\boldsymbol{\kappa}, \boldsymbol{\kappa}', E) = \langle \boldsymbol{\kappa}'|U_{\phi A,\phi A}|\boldsymbol{\kappa}\rangle = A\,\langle \boldsymbol{\kappa}', (\mathbf{p}_0 + \mathbf{q})|t_{\phi N,\phi N}(\omega_0)|\boldsymbol{\kappa}, \mathbf{p}_0\rangle\, F(q), \quad (78)$$

where $\mathbf{q} = \boldsymbol{\kappa} - \boldsymbol{\kappa}'$, $\mathbf{p}_0 = -\boldsymbol{\kappa}/A$, $\omega_0 = E_\phi(\kappa_0) + E_N(\kappa_0/A)$ with $\kappa_0$ defined by $E = E_\phi(\kappa_0) + E_A(\kappa_0)$, and

$$F(q) = \int d\mathbf{r} e^{i\mathbf{q}\cdot\mathbf{r}}\rho(\mathbf{r}). \quad (79)$$

Here $\rho(\mathbf{r})$ is the nuclear density normalized as $\int d\mathbf{r}\rho(\mathbf{r}) = 1$.

### A. Cross sections from the impulse term

By using the factorization approximation within the multiple-scattering formulation [34], the contribution from the impulse term $T^{\rm IMP}$ for spin $J = 0$ nuclei can be written as

$$\frac{d\sigma^{\rm IMP}}{d\Omega_{\rm Lab}} = \frac{(2\pi)^4|\mathbf{k}|^2 E_V(\mathbf{k})E_A(\mathbf{q}-\mathbf{k})}{|E_A(\mathbf{q}-\mathbf{k})|\mathbf{k}| + E_V(\mathbf{k})(|\mathbf{k}| - |\mathbf{q}|\cos\theta_{\rm Lab})|} \times |AF_T(t)\bar{t}(\mathbf{k},\mathbf{q})|^2, \quad (80)$$

where $t = (q-k)^2$ and $\bar{t}(\mathbf{k},\mathbf{q})$ is the spin-averaged $\gamma N \to VN$ amplitude defined by

$$|\bar{t}(\mathbf{k},\mathbf{q})|^2 = \frac{1}{4}\sum_{m_s,\lambda_\gamma}\sum_{m_s',\lambda_V} |\,\langle k\lambda_V; p_f m_s'|T_{VN,\gamma N}|q\lambda_\gamma; p_i m_s\rangle\,|^2. \quad (81)$$

Here, $\langle k\lambda_V; p_f m_s'|T_{VN,\gamma N}|q\lambda_\gamma; p_i m_s\rangle$ is the matrix element of the $\gamma(q) + N(p_i) \to V(k) + N(p_f)$ process as given in the previous section. The initial nucleon momentum $p_i$ in the initial target state is usually chosen as $p_i = (M_N, \mathbf{0})$ by the frozen nucleon approximation and the final nucleon momentum $p_f = (p_f^0, \mathbf{p}_f)$ is set as

$$\mathbf{p}_f = \mathbf{p}_i + (\mathbf{q} - \mathbf{k}),$$
$$p_f^0 = E_N(\mathbf{p}_f) = \sqrt{\mathbf{p}_f^2 + M_N^2}. \quad (82)$$

We follow the standard Hamiltonian formulation within which the $\gamma + N \to V + N$ process in nuclei can be off-energy shell, i.e., $q^0 + E_N(\mathbf{p}_i) \neq E_V(\mathbf{k}) + E_N(\mathbf{p}_f)$.

The factor $F_T(t)$ in Eq. (80) is a nuclear form factor which is probed by the gluon-exchange mechanism. Within the Pomeron-exchange model of Donnachie and Lanshoff [37], as used in Refs. [36,42], the same form factor is used in usual hadron-nuclear reactions and is defined as

$$F_T(t) = \langle\Psi_T|\sum_{i=1,A} e^{i\boldsymbol{\kappa}\cdot\mathbf{r}_i}|\Psi_T\rangle, \quad (83)$$

where $|\Psi_T\rangle$, normalized as $\langle\Psi_T|\Psi_T\rangle = 1$, is the nuclear ground state in the nuclear c.m. frame, and $\boldsymbol{\kappa}$ is related to $t$ by

$$-t = \boldsymbol{\kappa}^2 - \omega^2, \quad (84)$$

with

$$\omega = \sqrt{\boldsymbol{\kappa}^2 + M_T^2} - M_T. \quad (85)$$

Here $M_T$ is the mass of the target nucleus $T$. Clearly, $F_T(t)$ is related to the nuclear charge form factor $F_c(q^2)$ (with no exchange current contribution) by

$$F_c(q^2) = F_N(q^2)F_T(q^2 = t), \quad (86)$$

where $F_N(q^2)$ is the nucleon charge form factor.

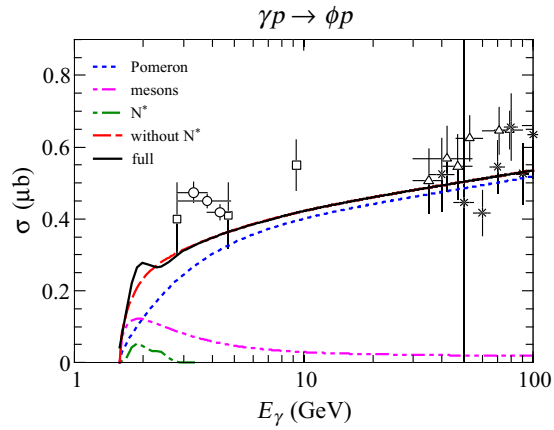


FIG. 7. Total cross section as a function of the photon energy in the laboratory frame $E_\gamma^{\rm lab}$. The blue dotted line stands for the Pomeron exchange only. The green dot-dashed and the magenta dot-dashed-dashed lines indicate the meson exchanges and $N^*$ contributions, respectively. The black solid and the red dashed lines represent the full contributions with and without $N^*$, respectively. The experimental data are from Refs. [56] (open squares), [57] (open circles), [58] (open triangles), and [59] (stars).

### B. Cross sections including final-state interaction

Including the FSI term, the differential cross sections are calculated as

$$\frac{d\sigma}{d\Omega_{\rm Lab}} = \frac{(2\pi)^4|\mathbf{k}|^2 E_V(\mathbf{k})E_A(\mathbf{q}-\mathbf{k})}{|E_A(\mathbf{q}-\mathbf{k})|\mathbf{k}| + E_V(\mathbf{k})(|\mathbf{k}| - |\mathbf{q}|\cos\theta_{\rm Lab})|} \times |AF_T(t)\bar{t}(\mathbf{k},\mathbf{q}) + T^{\rm FSI}(\mathbf{k},\mathbf{q},E)|^2, \quad (87)$$

where

$$T^{FSI}(\mathbf{k},\mathbf{q},E) = \int d\mathbf{k}' T_{\phi A,\phi A}(\mathbf{k},\mathbf{k}',E) \times \frac{AF(t')\bar{t}(\mathbf{k}',\mathbf{q})}{E - E_V(\mathbf{k}') - E_A(\mathbf{q}-\mathbf{k}') + i\epsilon}, \quad (88)$$

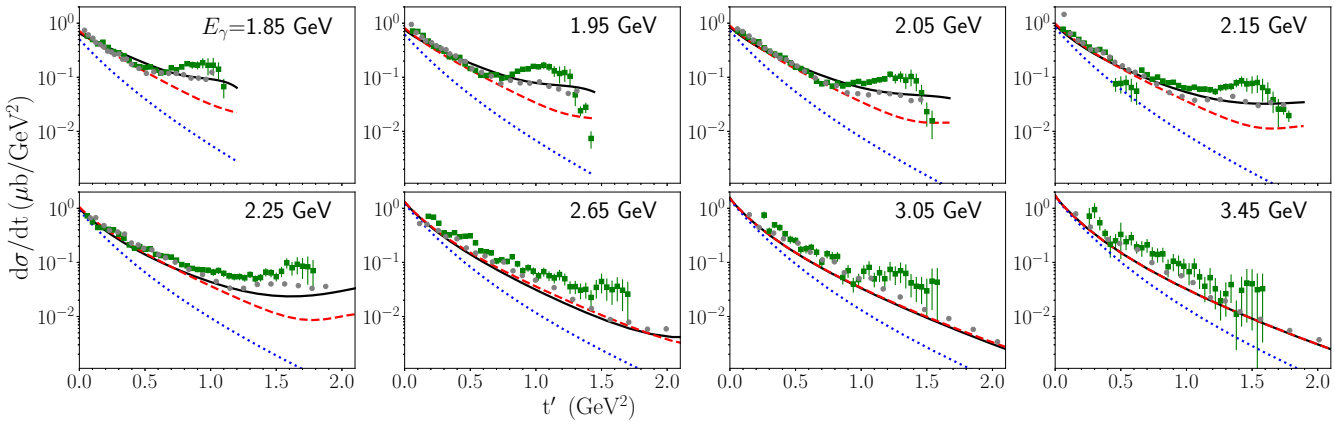


FIG. 8. Differential cross sections of $\gamma p \to \phi p$ without FSI at lower c.m. energies as functions of $t' = |t| - |t|_{\rm min}$. The blue dotted lines are from the calculations including Pomeron exchange only. The black solid lines and the red dashed lines represent the full contribution with and without $N^*$, respectively. The experimental data are from Ref. [53] (gray filled circles) and Ref. [60] (green filled squares).

with $t' = (q - k')^2$. It is most convenient to evaluate $t_{\phi A,\phi A}(\mathbf{k}, \mathbf{k}', E)$ in the $\phi A$ c.m. system, which leads to

$$T_{\phi A,\phi A}(\mathbf{k}, \mathbf{k}', E) = \sqrt{\frac{E_\phi(\boldsymbol{\kappa})E_A(-\boldsymbol{\kappa})}{E_\phi(\mathbf{k})E_A(\mathbf{k}+\mathbf{q})}}\, T_{\phi A,\phi A}(\boldsymbol{\kappa}, \boldsymbol{\kappa}', E) \times \sqrt{\frac{E_\phi(\boldsymbol{\kappa}')E_A(-\boldsymbol{\kappa}')}{E_\phi(\mathbf{k}')E_A(\mathbf{k}'+\mathbf{q})}}. \quad (89)$$

Here, $T_{\phi A,\phi A}(\boldsymbol{\kappa}, \boldsymbol{\kappa}', E)$ is calculated as

$$T_{\phi A,\phi A}(\boldsymbol{\kappa}, \boldsymbol{\kappa}', E) = U_{\phi A,\phi A}(\boldsymbol{\kappa}, \boldsymbol{\kappa}', E) + \int d\boldsymbol{\kappa}'' U_{\phi A,\phi A}(\boldsymbol{\kappa}, \boldsymbol{\kappa}'', E) \frac{1}{E - E_V(\boldsymbol{\kappa}'') - E_A(\boldsymbol{\kappa}'') + i\epsilon} \times T_{\phi A,\phi A}(\boldsymbol{\kappa}'', \boldsymbol{\kappa}', E). \quad (90)$$

## VI. RESULTS

In this section, we present and discuss our numerical results for the cross sections of $\gamma p \to \phi p$ and $\gamma\, ^4\mathrm{He} \to \phi\, ^4\mathrm{He}$.

### A. $\gamma p \to \phi p$

With the Pomeron-exchange model determined from the global fits to the total cross section data, as presented in Sec. III A, we first adjust the parameters of the meson-exchange and $N^*$ mechanisms to reproduce the CLAS data of Ref. [53]. To simplify the fit of the $N^*$ parameters, we use the relevant information from the results of Ref. [28]. The resulting parameters are shown and discussed in Sec. III D.

Our results on the differential cross sections of the $\gamma p \to \phi p$ reaction are presented in Fig. 6. This shows that the full results (black solid lines) of our model could explain the differential cross-section data of Ref. [53] very well. The Pomeron exchange (blue dotted lines) accounts for far forward angle regions and begins to deviate from the data as $\cos\theta$

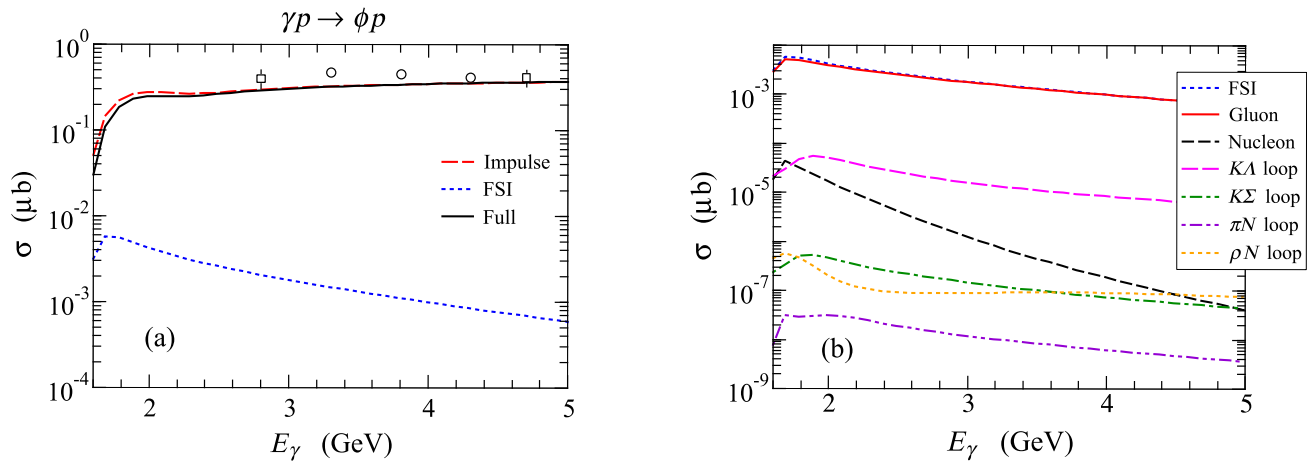


FIG. 9. Total cross sections of $\gamma p \to \phi p$ at low energies $E_\gamma$. (a) The red dashed and the blue dotted lines stand for the impulse and the FSI terms, respectively. The solid black line indicates the full contribution. The experimental data are from Refs. [56] (open squares) and [57] (open circles). (b) The individual contributions of the FSI terms.

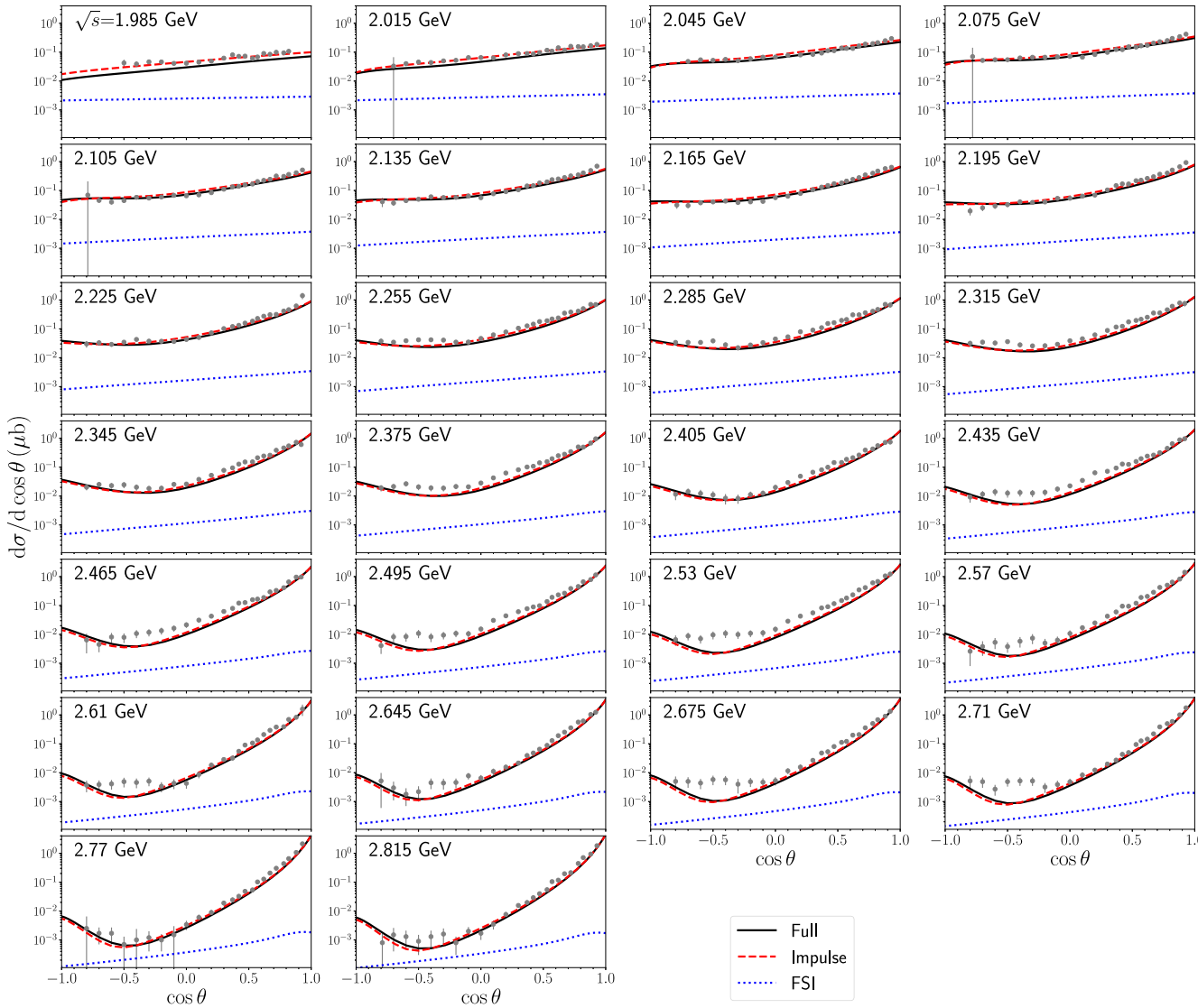


FIG. 10. Differential cross sections $d\sigma/d\cos\theta$ of the $\gamma p \to \phi p$ reaction as functions of $\cos\theta$ for different energies $\sqrt{s} = (1.985\text{–}2.815)$ GeV with and without the FSI effects. The red dashed and the blue dotted lines stand for the impulse and the FSI terms, respectively. The solid black lines indicate the full contributions. The experimental data are from the CLAS Collaboration [53].

decreases. The inclusion of various meson exchanges to the Pomeron exchange greatly enhances the results at $\cos\theta \geqslant 0$, as shown by green dot-dashed lines. The main meson-exchange effects are due to the exchanges of scalar mesons, i.e., $a_0$ and $f_0$ mesons. As shown by the red dashed lines, the direct $\phi$ radiation term is weak in the near threshold regions but becomes non-negligible as $\sqrt{s}$ $(=W)$ increases at large angles $\cos\theta \leqslant -0.5$. To reproduce the CLAS data more accurately at $2.0 \leqslant \sqrt{s} \leqslant 2.4$ GeV and at large angles, we need additional ingredients. We find that the $N^*$ excitations would play crucial roles in describing the data in these regions.

Figure 7 depicts the total cross section as a function of $E_\gamma$, the photon energy in the laboratory frame. This shows that the Pomeron-exchange (blue dotted line) is clearly the dominant mechanism in the high-energy region, $E_\gamma > 10$ GeV. However, in the near threshold region, the meson exchanges (magenta dot-dashed-dashed) and $N^*$ excitations (green dot-dashed) contribute sizable effects.

There are a few comments on $\phi$ photoproduction in low-energy region. In Fig. 8, we present the experimental data from Ref. [53] (gray filled circles) and from Ref. [60] (green filled squares) at $E_\gamma \leqslant 3.45$ GeV. This manifestly shows the inconsistency between these two data sets. In particular, the data of Ref. [60] have bump structures at large $t'$, while the structure is not seen or reduced in the data of Ref. [53]. As our model parameters are determined based on the data of Ref. [53], the bump structure cannot be simply reproduced by adjusting the meson exchanges and $N^*$ parameters in the present approach. Clearly, the differences between these two data sets need to be resolved before $N^*$ contributions can be more rigorously determined.

### B. $\gamma p \to \phi p$ with final-state interaction

With the model of the impulse approximation discussed in the previous section, we now consider the FSI in this section.

We present in Fig. 9(a) the result of the total cross sections of $\gamma p \to \phi p$ with the FSI effects. The impulse terms (red dashed lines) correspond to the full result in Fig. 7. The FSI effects represented by blue dotted lines are suppressed by factors of $10^2$–$10^3$ relative to the impulse terms in the considered photon energy region. The full results are given by the black solid lines, which are the sums of the impulse and FSI terms. This reveals a destructive interference effect between them at $E_\gamma \leqslant 2.4$ GeV.

Figure 9(b) displays the individual contributions of the FSI terms with the parameters determined in Sec. III. We find that the dominant contribution comes from the gluon-exchange interaction (red solid line) which is more than two orders of magnitudes larger than the contributions of other FSI terms. The $\phi N$ potential arising from the box diagrams depends on the cutoff parameters in the form factors. We choose $\Lambda_{MB}$ and $\Lambda'_{MB}$ in the range of the values used in the ANL-Osaka analysis of $\pi N$ and $\gamma N$ reactions [23]. The contributions of the box diagrams turn out to be rather weak. The $K\Lambda$-loop diagram (magenta long dashed line) is the dominant among the considered four box diagrams. The model parameters of the direct $\phi N$ coupling term (black short dashed line) [Figs. 2(b) and 2(c)] is determined from the $\phi$ radiation involved in the impulse term [Figs. 3(c) and 3(d)] using their similarities. The direct $\phi N$ coupling contribution is comparable to the contribution of the $K\Lambda$-loop diagram near the threshold $E_\gamma \simeq 2$ GeV but falls off faster as $E_\gamma$ increases.

In Fig. 10, we show the contributions from the FSI on differential cross sections $d\sigma/d\cos\theta$ as functions of $\cos\theta$. The impulse model (red dashed lines) corresponds to the full results of Fig. 6. This reveals that the FSI effects given by the blue dotted lines are clearly weak compared with the impulse terms over the whole scattering angles. Its shape is flat as a function of $\cos\theta$ near the threshold but becomes steeper as $\sqrt{s}$ increases.

For the gluon-exchange potential $\mathcal{V}_{\rm gluon} = -v_0 \exp(-\alpha r)/r$ of Eq. (52), we use $\alpha = 500$ MeV and $v_0 = 0.2$ which lie in the available ranges of $0.1 < v_0 < 1.0$ and $0.3 < \alpha < 0.6$ GeV. If we use a larger value for $v_0$, the full results (black solid lines) begin to deviate from the data near the threshold because the FSI term is destructive with the impulse term near the threshold region as indicated in Fig. 9(a). Meanwhile, they interfere constructively at rather high energies and at backward angles.

### C. $\gamma\,^4$He $\to \phi\,^4$He

In this section, we consider $\phi$ photoproduction from the $^4$He targets with the model for $\gamma p \to \phi p$ constructed in the present study. We first work with the model without FSI and then present our results with FSI. Presented in Fig. 11 are our results of differential cross sections $d\sigma/dt$ at $|t| = |t|_{\rm min}$. In this far forward region, the Pomeron-exchange contribution (dotted line) dominates, which can be expected. If we keep only Pomeron-exchange and meson-exchange terms in our calculations, i.e., if we neglect the $N^*$ contributions, we obtain the dashed line which somehow overestimates the experimental data [14]. Although the $N^*$ contributions (dash-dotted line) are much weaker than the other mechanisms, inclusion of the

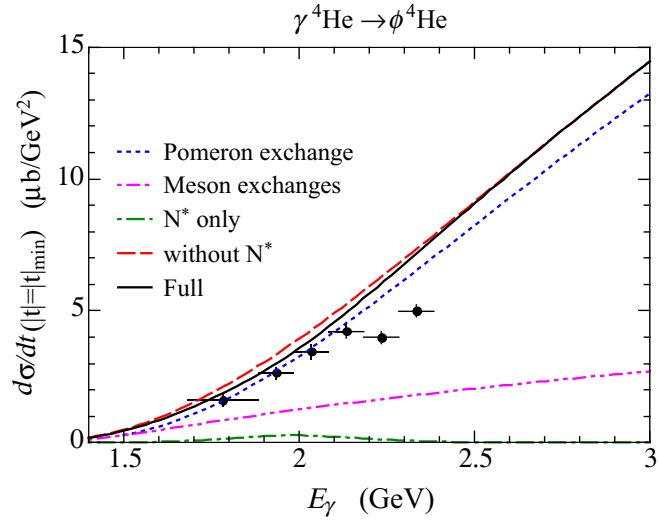


FIG. 11. Differential cross sections $d\sigma/dt$ at $t = t_{\rm min}$ as a function of $E_\gamma$ for the reaction of $\gamma\,^4$He $\to \phi\,^4$He. The experimental data are from the LEPS Collaboration [14].

$N^*$ results in a better description of the experimental data of LEPS Collaboration [14] in the region of $E_\gamma < 2.2$ GeV as shown by the solid line. This observation is ascribed to the fact that the $N^*$ contributions interfere destructively with the other terms. However, the structure shown by the experimental data at $E_\gamma \geqslant 2.2$ GeV cannot be explained by our model calculations with variation of parameters.

In Fig. 12, we show differential cross sections $d\sigma/dt$ as functions of $t' \equiv |t| - |t|_{\rm min}$ for photon energies from 1.685 to 2.385 GeV. We find that, in this forward angle region, the slopes of the dominant Pomeron exchange (dotted lines) match very well with the experimental data. The calculated magnitudes of our full calculations (solid lines) are also in a reasonable agreement with the data, indicating that

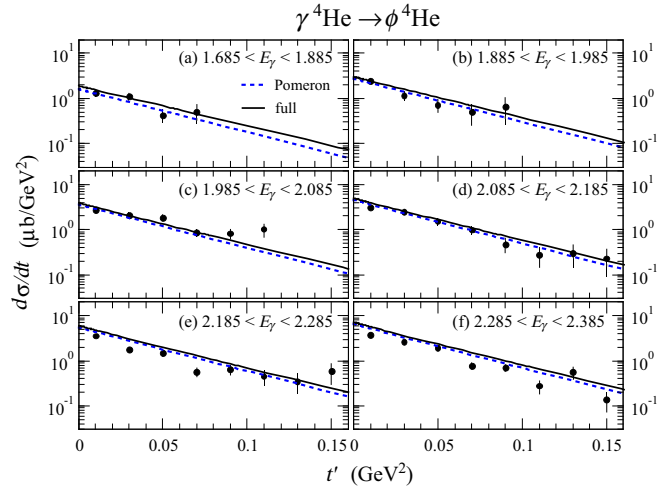


FIG. 12. Differential cross sections $d\sigma/dt$ of $\gamma\,^4$He $\to \phi\,^4$He as functions of $t' \equiv |t| - |t|_{\rm min}$ at $1.685 < E_\gamma < 2.385$ GeV. The dotted lines and the solid lines stand for the Pomeron and full contributions, respectively. The experimental data are from Ref. [14].

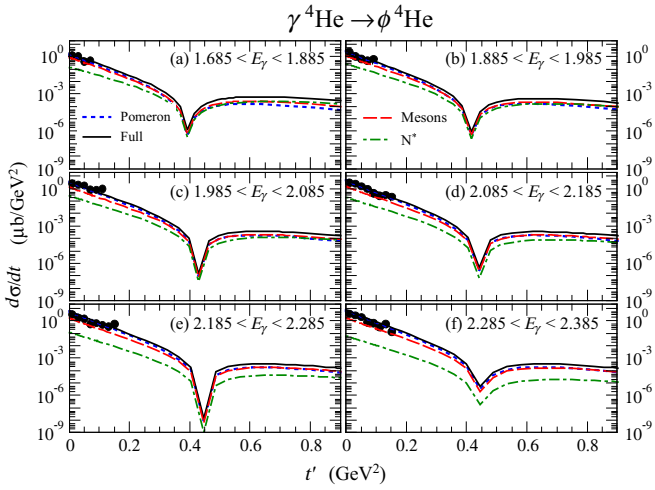


FIG. 13. Same as Fig. 12 but for a wider range of $t' = |t| - |t|_{\min}$. The dotted lines and the solid lines stand for the Pomeron and full contributions, respectively. The dot-dashed lines are from the $N^*$ contributions. The experimental data are from Ref. [14].

contributions from meson exchanges and $N^*$ contributions are small in this far forward angle region. Their contributions become more sizable, however, at larger scattering angles, as shown in Fig. 13, which also shows differential cross sections for a wider range of $t'$. The bump structures shown at $t' \approx 0.4$ GeV$^2$ in Fig. 13 are due to the structure of the form factor $F_T(t)$ as seen in Eqs. (87) and (88). This structure could be tested in a future experiment.

The results for $\phi$ photoproduction from the $^4$He targets discussed so far are based on the impulse approximation for $\gamma p \to \phi p$. We also carry out the calculations with FSI and our numerical results are presented in Fig. 14, which shows the results up to $t' = 3$ GeV$^2$. Here, we can see that the

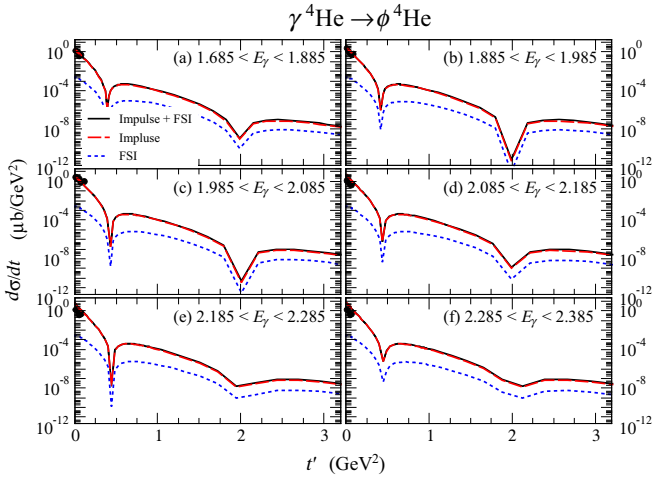


FIG. 14. Same as Fig. 13 but for a wider range of $t' = |t| - |t|_{\min}$. The dotted lines are the results with impulse approximation and FSI contributions are shown by the dashed lines. Their sums are given by the solid lines. The experimental data are from Ref. [14].

FSI contributions (dotted lines) are very weak. This is not surprising since the FSI effects are already very small for the production of the $\phi$ meson on the proton target, as shown in Fig. 10. Furthermore, it is further reduced by the nuclear form factor $F(q)$ in the optical potential defined in Eq. (78).

## VII. SUMMARY AND CONCLUSION

In this work, we have investigated $\phi$ photoproduction on nucleon targets and $^4$He targets based on the approach developed by the ANL-Osaka collaboration group [23]. The starting point is to construct a Hamiltonian which describes the mechanisms of $\phi$ photoproduction by the Pomeron-exchange, meson-exchange, $\phi$-radiation, and $N^*$-excitation processes. The final $\phi N$ interactions are described by the gluon-exchange and the direct $\phi N$ coupling as well as the box diagram arising from the $\pi N$, $\rho N$, $K\Lambda$, and $K\Sigma$ channels. The parameters of the Hamiltonian are determined by fitting the data of $\gamma p \to \phi p$ [53]. The resulting Hamiltonian is then used to predict the coherent $\phi$ production on the $^4$He targets by using the distorted-wave impulse approximation.

For the proton target, we find that the Pomeron-exchange contributions are dominant in the very forward angles and the meson-exchange mechanisms are crucial in obtaining a good fit to the experimental data in the large scattering angles, where the $N^*$ excitations and $\phi$ radiation mechanisms are also required to describe the data at the considered energy region. The final $\phi N$ rescattering effects, as required by the unitarity condition, are found to be very weak and the model without the FSI effects is enough to reasonably describe the data.

For the $^4$He target, the calculated differential cross sections are in a very good agreement with the LEPS data [14] at low energies and for forward-scattering angles. The FSI effects are also found to be negligible because of the further suppression originated from the nuclear form factor. The bump structures predicted by the present work could be tested by future experiments at a wider range of scattering angles. However, the structure observed by the LEPS collaboration on $d\sigma/dt$ for the far forward region at $E_\gamma \approx 2.2$–$2.4$ GeV could not be explained by the present exploratory model and deserves further studies both in experiment and in theory.

On the other hand, in the energy region considered, it would be interesting to investigate the role of other higher energy meson-baryon channels, such as $\pi\Delta$, $\rho\Delta$, and $K\Lambda^*$, by extending the present work. In addition, a full scale coupled-channels calculation as what was done by the ANL-Osaka Collaboration could be carried out to go beyond the box-diagram approximations. Our efforts in these directions will be reported elsewhere.

## ACKNOWLEDGMENTS

S.-H.K. and Y.O. are grateful to K. Tsushima for useful discussions at the early stage of this work. S.-H.K. also thanks T. Hiraiwa for providing the experimental data. The work of S.-H.K. was supported by National Research Foundation (NRF) of Korea under Grants No. NRF-2019R1C1C1005790 and No. NRF-2021R1A6A1A03043957. S.i.N. was supported

by NRF under Grants No. NRF-2018R1A5A1025563 and No. NRF-2019R1A2C1005697. T.-S.H.L. was supported by the Office of Science of the U.S. Department of Energy under Contract No. DE-AC02-05CH1123. The research of Y.O. was supported by Kyungpook National University Research Fund, 2021.

[1] L. Stodolsky, Hadronic Behavior of $\gamma$, $\nu$-Nuclear Cross Sections, Phys. Rev. Lett. **18**, 135 (1967).
[2] T. H. Bauer, R. D. Spital, D. R. Yennie, and F. M. Pipkin, The hadronic properties of the photon in high-energy interactions, Rev. Mod. Phys. **50**, 261 (1978), **51**, 407(E) (1979).
[3] W. Weise, Hadronic aspects of photon-nucleus interactions, Phys. Rep. **13**, 53 (1974).
[4] G. Grammer, Jr. and J. D. Sullivan, Nuclear shadowing of electromagnetic processes, in *Electromagnetic Interactions of Hadrons*, edited by A. Donnachie and G. Shaw (Plenum Press, New York, 1978), Vol. 2, pp. 195–352.
[5] B. Krusche, Photoproduction of mesons off nuclei. Electromagnetic excitations of the neutron and meson-nucleus interactions, Eur. Phys. J. Spec. Top. **198**, 199 (2011).
[6] G. E. Brown and M. Rho, Scaling Effective Lagrangians in a Dense Medium, Phys. Rev. Lett. **66**, 2720 (1991).
[7] G. McClellan, N. Mistry, P. Mostek, H. Ogren, A. Osborne, J. Swartz, R. Talman, and G. Diambrini-Palazzi, Photoproduction of $\phi^0$ Mesons from Hydrogen, Deuterium, and Complex Nuclei, Phys. Rev. Lett. **26**, 1593 (1971).
[8] T. Ishikawa *et al.*, $\phi$ photo-production from Li, C, Al, and Cu nuclei at $E_\gamma = 1.5$–$2.4$ GeV, Phys. Lett. B **608**, 215 (2005).
[9] T. Mibe *et al.* (CLAS Collaboration), Measurement of coherent $\phi$-meson photoproduction from the deuteron at low energies, Phys. Rev. C **76**, 052202(R) (2007).
[10] W. C. Chang *et al.* (LEPS Collaboration), Forward coherent $\phi$-meson photoproduction from deuterons near threshold, Phys. Lett. B **658**, 209 (2008).
[11] W. C. Chang *et al.* (LEPS Collaboration), Measurement of the incoherent $\gamma d \to \phi pn$ photoproduction near threshold, Phys. Lett. B **684**, 6 (2010).
[12] W. C. Chang *et al.*, Measurement of spin-density matrix elements for $\phi$-meson photoproduction from protons and deuterons near threshold, Phys. Rev. C **82**, 015205 (2010).
[13] X. Qian *et al.* (CLAS Collaboration), Near-threshold photoproduction of $\phi$ mesons from deuterium, Phys. Lett. B **696**, 338 (2011).
[14] T. Hiraiwa *et al.* (LEPS Collaboration), First measurement of coherent $\phi$-meson photoproduction from $^4$He near threshold, Phys. Rev. C **97**, 035208 (2018).
[15] T. Hiraiwa, Ph.D. thesis, Kyoto University, 2018 (unpublished).
[16] A. I. Titov, M. Fujiwara, and T.-S. H. Lee, Coherent $\phi$ and $\omega$ meson photoproduction from deuteron and nondiffractive channels, Phys. Rev. C **66**, 022202(R) (2002).
[17] T. C. Rogers, M. M. Sargsian, and M. I. Strikman, Coherent vector meson photoproduction from deuterium at intermediate energies, Phys. Rev. C **73**, 045202 (2006).
[18] A. I. Titov and B. Kämpfer, Photoproduction of the $\phi$ meson off the deuteron near threshold, Phys. Rev. C **76**, 035202 (2007).
[19] T. Sekihara, A. Martınez Torres, D. Jido, and E. Oset, Theoretical study of incoherent $\phi$ photoproduction on a deuteron target, Eur. Phys. J. A **48**, 10 (2012).
[20] A. J. Freese and M. M. Sargsian, Probing vector mesons in deuteron breakup reactions, Phys. Rev. C **88**, 044604 (2013).
[21] A. Kiswandhi, S. N. Yang, and Y. B. Dong, Near-threshold incoherent $\phi$ photoproduction on the deuteron: Searching for traces of a resonance, Phys. Rev. C **94**, 015202 (2016).
[22] A. Matsuyama, T. Sato, and T.-S. H. Lee, Dynamical coupled-channel model of meson production reactions in the nucleon resonance region, Phys. Rep. **439**, 193 (2007).
[23] H. Kamano, T.-S. H. Lee, S. X. Nakamura, and T. Sato, The ANL-Osaka partial-wave amplitudes of $\pi N$ and $\gamma N$ reactions, arXiv:1909.11935.
[24] J. M. Laget, Exclusive meson photo- and electro-production, a window on the structure of hadronic matter, Prog. Part. Nucl. Phys. **111**, 103737 (2020).
[25] A. I. Titov, Y. Oh, and S. N. Yang, Polarization Observables in $\phi$ Meson Photoproduction and the Strangeness Content of the Proton, Phys. Rev. Lett. **79**, 1634 (1997).
[26] A. I. Titov, Y. Oh, S. N. Yang, and T. Morii, Photoproduction of $\varphi$ meson from proton: Polarization observables and the strangeness in the nucleon, Phys. Rev. C **58**, 2429 (1998).
[27] A. I. Titov, T.-S. H. Lee, H. Toki, and O. Streltsova, Structure of the $\varphi$ photoproduction amplitude at a few GeV, Phys. Rev. C **60**, 035205 (1999).
[28] S.-H. Kim and S.-I. Nam, Pomeron, nucleon-resonance, and $(0^+, 0^-, 1^+)$-meson contributions in $\phi$-meson photoproduction, Phys. Rev. C **100**, 065208 (2019).
[29] S.-H. Kim and S.-I. Nam, Investigation of electroproduction of $\phi$ mesons off protons, Phys. Rev. C **101**, 065201 (2020).
[30] F. Huang, M. Döring, H. Haberzettl, J. Haidenbauer, C. Hanhart, S. Krewald, U.-G. Meißner, and K. Nakayama, Pion photoproduction in a dynamical coupled-channels model, Phys. Rev. C **85**, 054003 (2012).
[31] A. V. Anisovich, R. Beck, E. Klempt, V. A. Nikonov, A. V. Sarantsev, and U. Thoma, Properties of baryon resonances from a multichannel partial wave analysis, Eur. Phys. J. A **48**, 15 (2012).
[32] R. A. Arndt, W. J. Briscoe, R. L. Workman, and I. I. Strakovsky, Partial-Wave Analysis Facility (SAID); https://gwdac.phys.gwu.edu
[33] S. R. Beane, E. Chang, S. D. Cohen, W. Detmold, H.-W. Lin, K. Orginos, A. Parreño, and M. J. Savage (NPLQCD Collaboration), Quarkonium-nucleus bound states from lattice QCD, Phys. Rev. D **91**, 114503 (2015).
[34] H. Feshbach, *Theoretical Nuclear Physics: Nuclear Reactions* (John Wiley and Sons, Inc., New York, 1992).
[35] M. L. Goldberger and K. M. Watson, *Collision Theory* (John Wiley and Sons, Inc., New York, 1964).
[36] J.-J. Wu and T.-S. H. Lee, Photoproduction of bound states with hidden charm, Phys. Rev. C **86**, 065203 (2012).
[37] A. Donnachie and P. V. Landshoff, Elastic scattering and diffraction dissociation, Nucl. Phys. B **244**, 322 (1984).
[38] A. Donnachie and P. V. Landshoff, Dynamics of elastic scattering, Nucl. Phys. B **267**, 690 (1986).
[39] A. Donnachie and P. V. Landshoff, Exclusive rho production in deep inelastic scattering, Phys. Lett. B **185**, 403 (1987).
[40] A. Donnachie and P. V. Landshoff, Total cross sections, Phys. Lett. B **296**, 227 (1992).

[41] Y. Oh, A. I. Titov, and T.-S. H. Lee, Nucleon resonance in $\omega$ photoproduction, Phys. Rev. C **63**, 025201 (2001).
[42] Y. Oh and T.-S. H. Lee, One-loop corrections to $\omega$ photoproduction near threshold, Phys. Rev. C **66**, 045201 (2002).
[43] P. A. Zyla *et al.*, Particle data group, the review of particle physics, Prog. Theor. Exp. Phys. **2020**, 083C01 (2020).
[44] M. A. Pichowsky and T.-S. H. Lee, Exclusive diffractive processes and the quark substructure of mesons, Phys. Rev. D **56**, 1644 (1997).
[45] Y. Oh and T.-S. H. Lee, $\rho$ meson photoproduction at low energies, Phys. Rev. C **69**, 025201 (2004).
[46] E. Maguire, L. Heinrich, and G. Watt, HEPData: A repository for high energy physics data, J. Phys.: Conf. Ser. **898**, 102006 (2017).
[47] V. G. J. Stoks and Th. A. Rijken, Soft-core baryon-baryon potentials for the complete baryon octet, Phys. Rev. C **59**, 3009 (1999).
[48] Th. A. Rijken, V. G. J. Stoks, and Y. Yamamoto, Soft-core hyperon-nucleon potentials, Phys. Rev. C **59**, 21 (1999).
[49] M. Birkel and H. Fritzsch, Nucleon spin and the mixing of axial vector mesons, Phys. Rev. D **53**, 6195 (1996).
[50] N. I. Kochelev, D.-P. Min, Y. Oh, V. Vento, and A. V. Vinnikov, New anomalous trajectory in Regge theory, Phys. Rev. D **61**, 094008 (2000).
[51] U.-G. Meißner, V. Mull, J. Speth, and J. W. Van Orden, Strange vector currents and the OZI-rule, Phys. Lett. B **408**, 381 (1997).
[52] R. M. Davidson and R. Workman, Form factors and photoproduction amplitudes, Phys. Rev. C **63**, 025210 (2001).
[53] B. Dey *et al.* (CLAS Collaboration), Data analysis techniques, differential cross sections, and spin density matrix elements for the reaction $\gamma p \to \phi p$, Phys. Rev. C **89**, 055208 (2014).
[54] T. Kawanai and S. Sasaki, Charmonium-nucleon potential from lattice QCD, Phys. Rev. D **82**, 091501(R) (2010).
[55] H. Gao, T. S. H. Lee, and V. Marinov, $\phi$-$N$ bound state, Phys. Rev. C **63**, 022201(R) (2001).
[56] J. Ballam *et al.*, Vector-meson production by polarized photons at 2.8, 4.7, and 9.3 GeV, Phys. Rev. D **7**, 3150 (1973).
[57] D. P. Barber *et al.*, A study of elastic photoproduction of low mass $K^+K^-$ pairs from hydrogen in the energy range 2.8–4.8 GeV, Z. Phys. C: Part. Fields **12**, 1 (1982).
[58] R. M. Egloff *et al.*, Measurements of Elastic $\rho$- and $\phi$-Meson Photoproduction Cross Sections on Protons from 30 to 180 GeV, Phys. Rev. Lett. **43**, 657 (1979).
[59] J. Busenitz *et al.*, High-energy photoproduction of $\pi^+\pi^-\pi^0$, $K^+K^-$, and $p\bar{p}$ states, Phys. Rev. D **40**, 1 (1989).
[60] H. Seraydaryan *et al.* (CLAS Collaboration), $\phi$-meson photoproduction on hydrogen in the neutral decay mode, Phys. Rev. C **89**, 055206 (2014).